RESEARCH PAPER

Cancer Biology & Therapy 12:4, 1-8; August 15, 2011; © 2011 Landes Bioscience

Combination of ultrasound and bubble liposome enhance the effect of doxorubicin and inhibit murine osteosarcoma growth

Yoshinori Ueno,[1,†] Shozo Sonoda,[2,†] Ryo Suzuki,[3] Masahiro Yokouchi,[1,*] Yasuomi Kawasoe,[1] Katsuro Tachibana,[4] Kazuo Maruyama,[3] Taiji Sakamoto[2] and Setsuro Komiya[1]

[1]Department of Orthopaedic Surgery; [2]Department of Ophthalmology; Graduate School of Medical and Dental Sciences; Kagoshima University; Kagoshima; [3]Department of Biopharmaceutics; School of Pharmaceutical Sciences; Teikyo University; Kanagawa; [4]Department of Anatomy; Fukuoka University School of Medicine; Fukuoka, Japan

[†]These authors equally contributed to this work.

Keywords: bubble liposome (BL), ultrasound, doxorubicin, sonoporation, cavitation, osteosarcoma, drug delivery system (DDS)

If ultrasound (US) is applied to cells, permeability across the cell membrane temporarily increases, making it easier for drugs to be taken into the cells from around the cell membrane. Moreover, when used in combination with Bubble liposome (BL: liposomes which entrap an ultrasound imaging gas), even low-power ultrasound can facilitate drug delivery into cells.

In the present study, we constructed a new drug delivery system (DDS) involving concomitant use of US and BL with doxorubicin (DOX), a key drug in the chemotherapy of osteosarcoma, and demonstrated both in vitro and in vivo that it markedly inhibited the proliferation of osteosarcoma cells. Furthermore, this system achieved an equivalent antitumor effect at about 1/5 the dose of antitumor agent employed in monotherapy with DOX. These findings suggest the possibility of reduction of adverse events.

In this experiment, US and liposomes were tested, both of which are already in use in clinical practice. US and liposomes are both very safe in the body. The DDS composed of these elements we designed can be applied in simple and site-specific fashion and is therefore promising as a new, clinically feasible method of treatment.

Introduction

Osteosarcoma is the most frequent primary malignant bone tumor. Because of early pulmonary spread, this tumor had a miserable prognosis prior to the availability of chemotherapy. Currently, among the available cytostatic drugs, the four agents methotrexate, ifosfamide, cisplatinum and doxorubicin (DOX, adriamycin) are considered most effective.[1-3] Thus, the identification of effective neoadjuvant chemotherapy in combination with surgery for osteosarcoma patients has led to a significant improvement in outcome in recent decades.

However, there are still a certain number of patients who do not benefit from these improvements. Despite advancements in multimodality treatment consisting of aggressive chemotherapy, metastasis develops in more than one-third of patients, 90% of whom rarely respond to salvage treatment. Chemotherapeutic regimens require high dosages of agents to successfully eliminate tumor, adversely affecting healthy tissues in the host. The side effects of many antineoplastic agents include cardiotoxicity, immune suppression, nephrotoxicity and others.[4,5] It is therefore believed that alternative strategies for the treatment of osteosarcoma are necessary.

Microbubbles (MB), which are contrast agents for medical ultrasound (US) imaging, improve the efficiency of transfection through US-induced cavitation.[6-11] Microbubbles are, however, generally unstable, and their mean diameter of about 1–6 μm is too large for extravascular applications.[12] It is difficult to add modified products such as functional ligaments to the surface of MB. Therefore, MB should generally be smaller than red blood cells and stable after injection into the blood circulation, and ultimately their surface should be easily modifiable with functional molecules for targeting.

Liposomes have certain advantages as drug, antigen or gene delivery carriers.[13-18] Their size is easily varied, and they can be modified to add a targeting function. Based on liposome technology, we have developed novel liposomal bubbles (Bubble liposome (BL) which were liposomes containing the US imaging gas perfluoropropane).[19] In our system, DOX and BL were simply mixed rather than sealing DOX inside of liposomes. And we reported that the combination of BL and US irradiation could be

*Correspondence to: Masahiro Yokouchi; Email: masahiro@m3.kufm.kagoshima-u.ac.jp
Submitted: 12/09/10; Revised: 04/04/11; Accepted: 05/03/11
DOI:

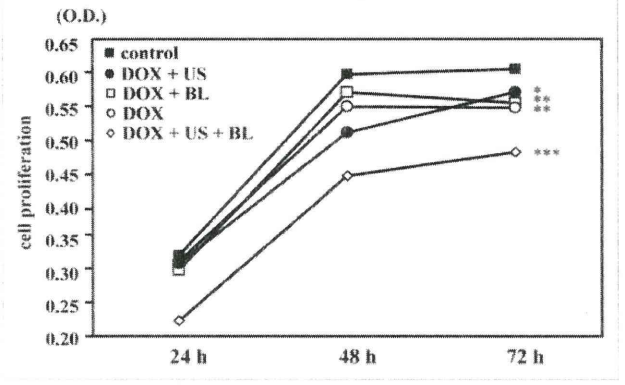

Figure 1. BL and US, used separately or in combination, facilitate drug uptake by cells. The effect of combined use of BL and US was investigated by assessing DOX-induced suppression of LM8 cell proliferation. LM8 cell proliferation was determined using MTT assay. Cell viability decreased significantly followed application of BL + US + DOX ($p < 0.001$).

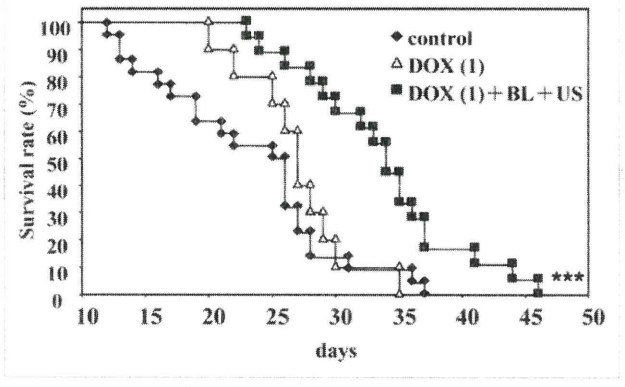

Figure 2. Kaplan-Meier survival curves show the effects of BL and US on the survival of mice bearing osteosarcoma. The DOX + BL + US group (n = 18) exhibited significant differences in survival compared with the DOX-alone group (n = 10) and control group (n = 22) ($p < 0.001$).

utilized as gene (plasmid DNA and siRNA) and antigen delivery systems.[20-24]

We used DOX in this study and designed a new drug delivery system (DDS) using BL for the development of a new and alternative approach to the treatment of osteosarcoma. In the present study, the anti-tumor effects of the new DDS using DOX in murine osteosarcoma cells in vivo and in vitro were investigated.

Results

Cytotoxicity of BL and US to LM8 cells. In the group that received no treatment (control), optical density increased to about 0.6 at 48–72 h. The value in the group receiving DOX with US irradiation was significantly different from the control ($p < 0.05$). In the groups receiving DOX with BL, receiving DOX alone, values were significantly different from the control ($p < 0.01$). In the groups receiving DOX combined with BL and US irradiation, values were significantly different from the control ($p < 0.001$) (**Fig. 1**). It was confirmed that the effect of DOX was markedly enhanced by combining it with BL and US.

Tumor growth delay. We examined whether a tumor suppressive effect could be observed with the combination of BL and US in vivo as in vitro. In the control group, the tumors increased rapidly and liver metastasis, renal metastasis and ascites were noted on day 21, and 50% of individuals died by day 25 (**Fig. 2**). In the control group, normalized tumor volume rapidly increased throughout the experiment (42.4 ± 6.3) (**Fig. 3A and B**). In the groups receiving US irradiation or BL treatment alone or US with BL treatment, normalized tumor volume was suppressed throughout the experiment (US: 22.7 ± 6.9, BL: 29.6 ± 7.5, US + BL: 21.7 ± 4.5), though without significant differences from control group ($p > 0.05$) (**Fig. 3A**). In the groups receiving DOX treatment alone at a concentration of 1.0 mg/kg with or without US irradiation, tumor volume was suppressed compared with the control group (DOX (1): 22.4 ± 2.8, DOX (1) + US: 27.8 ± 1.9), though not to a significant extent compared with control group ($p > 0.05$). With BL combined with DOX and US treatment, there was clear tumor suppression even at low concentrations of 1.0 mg/kg (DOX (1) + BL + US: 8.3 ± 2.8) ($p < 0.001$) (**Fig. 3B and C**), with effectiveness of suppression equivalent to that with five times the dose of DOX (DOX (5): 7.8 ± 1.4) (**Fig. 3B**). The survival rate of mice treated with DOX (1) + BL + US was higher than that of mice treated with the same concentration of DOX (1) alone (**Fig. 2**). Thus, as in previous studies of MB, drug uptake was increased with use of BL combined with US irradiation and a tumor suppressive effect was confirmed.

Evaluation of side effect. **Table 1** shows blood counts and liver function parameters in mice. There were no significant differences among the groups in WBC, RBC, GOT or GPT. The Hb value of mice receiving DOX (5 mg/kg) alone was statistically different from the control value. Mice receiving DOX alone at concentrations of 1.0 mg/kg or 5.0 mg/kg had Plt values significantly different from the control group. In contrast, mice receiving DOX (1 mg/kg) combined with BL and US exhibited no significant differences from the control group in blood counts and liver function.

Assay for intratumoral DOX content. Previous studies suggested that the effect of treatment with BL combined with US was due to induction of permeability of the cell membrane by US irradiation. To demonstrate this, we examined intratumoral DOX content. Mean concentration of DOX + BL + US tumors showed a significant differences compared with DOX alone group and showed a 57% (1.95 $\mu g\ g^{-1}$/1.24 $\mu g\ g^{-1}$) increase in DOX alone group ($p < 0.05$) (**Fig. 4A**). DOX uptake by cells was thus increased by the combination of BL and US.

Discussion

In the present study, we constructed a new DDS by concomitant use of US and BL with DOX, a key drug in the chemotherapy of osteosarcoma and demonstrated both in vitro and in vivo that this DDS markedly inhibited the proliferation of osteosarcoma cells. Furthermore, this system achieved an equivalent antitumor

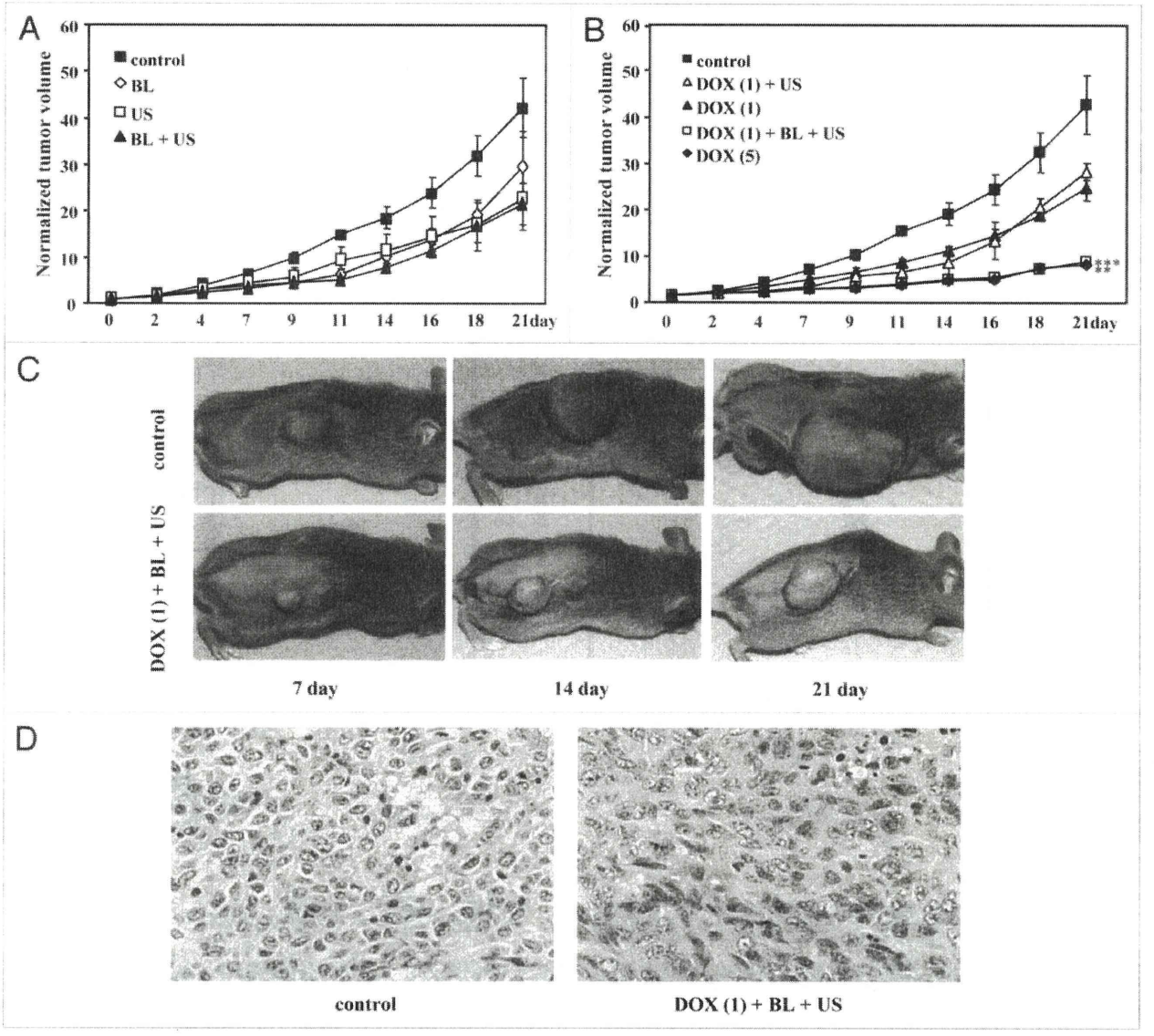

Figure 3. Tumor growth delay. (A) The anti-tumor effects of DOX were assessed by comparing the normalized tumor volume of (■) controls with (◇) the group administered BL alone, (■) the group administered US alone and (◆) the group administered BL in combination with US. There were no significant differences among the groups. (B) The anti-tumor effects of DOX were assessed by comparing the normalized tumor volume of (■) controls with (△) the group administered DOX (1) in combination with US, (▲) the group administered DOX (1) alone, (■) the group that received DOX (1) in combination with BL and US, and (◆) the group administered DOX (5) alone. The DOX (1) + BL + US group exhibited a significant difference in tumor volume from the control group ($p < 0.001$). (C) Examples of visual observation of tumor growth in the mouse model. A representative animal from each group is shown. The upper part shows control. The lower part shows the group treated with DOX (1) in combination with BL and US. The left part shows the mice at day 7, the middle part at day 14 and the right part at day 21. (D) H&E staining of LM8 tumor cells excised on day 21. H&E staining of tumor samples from (left part) the control group and (right part) the group treated with DOX, BL and US. There were no marked differences between the two groups in cell morphology. Magnification, x400. DOX (1) = received DOX at 1 mg/kg body weight, DOX (5) = received DOX at 5 mg/kg body weight.

effect at about 1/5 the dose of antitumor agent employed in monotherapy with DOX. These findings suggest the possibility of reduction of adverse events in the host.

The greatest advantage of use of a liposome preparation for drug delivery application is that the liposome itself is a drug whose safety has been established. Furthermore, it is easy to add modified products such as functional ligands to the surface of liposomes. However, problems with liposomes have included the instability of crude liposomes in the body and their uptake by the reticular endothelial system (RES) including the liver, spleen after intravenous administration. To solve these problems, which have hampered the clinical use of liposomes,

Table 1. Complete blood count and liver function enzyme assay

	WBC	RBC	Hb	plt	GOT	GPT
contorol	4260 ± 901	731 ± 46	12.86 ± 0.55	74.76 ± 12.82	59.0 ± 15.79	27.0 ± 4.06
DOX (1)	5020 ± 766	630 ± 133	11.18 ± 2.23	50.02 ± 2.92*	68.2 ± 17.69	33.4 ± 5.45
DOX (1) + BL + US	4460 ± 867	654 ± 123	11.84 ± 1.58	63.14 ± 8.40	61.8 ± 11.56	31.6 ± 4.82
DOX (5)	3740 ± 1504	588 ± 164	9.92 ± 2.48**	33.08 ± 13.37**	73.6 ± 21.51	37.6 ± 18.79

Hb level decreased in the uncombined DOX (5) treatment group ($p < 0.05$). Plt count decreased significantly in the uncombined DOX (1) treatment group ($p < 0.05$) and the uncombined DOX (5) treatment group ($p < 0.01$). No significant difference was noted in any parameter between the BL + US group and the control group.

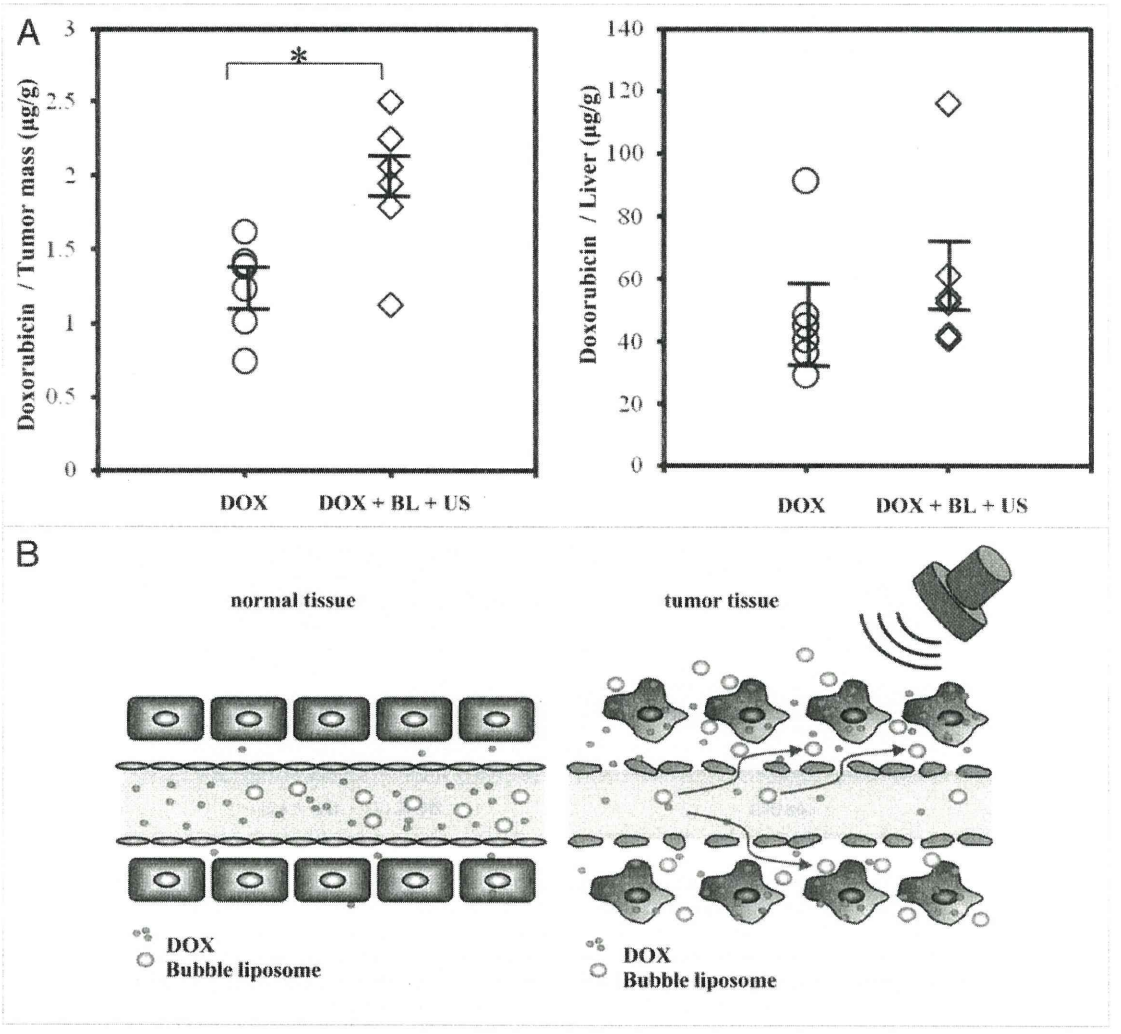

Figure 4. (A) Assay for DOX Content. Intratumoral DOX level (left part) and liver tissue DOX level (right part) were compared between mice that received injection of DOX alone and mice that received DOX in combination with BL and US. Intratumoral DOX level was significantly higher in the DOX + BL + US group than in the uncombined DOX injection group ($p < 0.05$). Liver tissue DOX level did not differ significantly between the two groups. (B) *EPR effect.* According to the anatomical and pathophysiological abnormalities of tumor tissues, biocompatible macromolecules and lipids will spontaneously and preferentially leak from tumor vessels into tumor tissues due to increased microvessel permeability and be retained in the tumor for extended periods of time due to poor lymph drainage.

polyethylene glycol (PEG) liposomes that could evade the RES as a result of modification of their surface with PEG were developed.[25-27] Because of its persistent enhanced permeability and retention (EPR) effect, the long-term retention-type liposome with PEG has been demonstrated to yield higher accumulation in tumors.[28,29] This type of targeting is called "passive

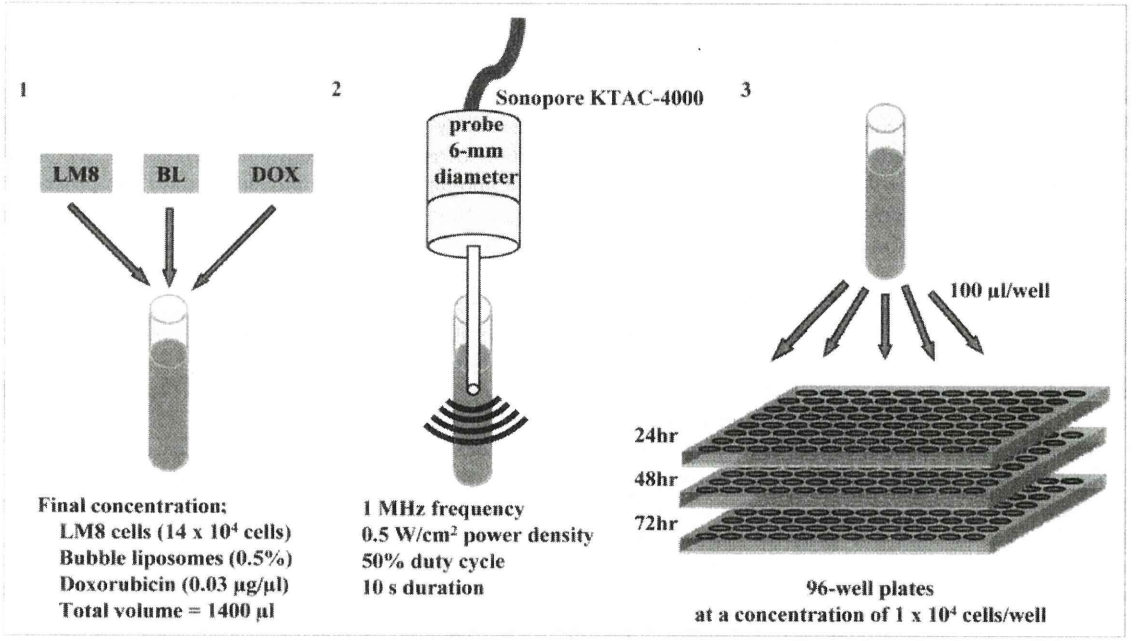

Figure 5. Method of in vitro experiment for evaluation of the effectiveness of BL and US in LM8 cells. (1) LM8 cells, BL and DOX are combined, followed by filling to a total volume of 1,400 µl (final concentration: LM8 cells (14 x 10^4 cells), BLs (0.5%), DOX (0.03 µg/µl)). (2) US is immediately applied to the mixture. (3) A 96-well plate is inoculated and cell viability is measured by MTT assay 24, 48 and 72 h later.

targeting" and serves as the basis of treatment strategies using liposomes. With the progress in research on targeting, such as passive targeting as described above, research on active targeting has also proceeded. The latter aims at targeting by liposomes to which functional ligands such as antibodies are bound and at the enhancement of drug uptake using additive application.[30-32] Concerning active targeting using DOX, there are reports on tumor inhibitory effects obtained through the concurrent use of thermosensitive liposomal DOX and hyperthermia,[32] and tumor inhibition through the use of small magnetic liposomes containing DOX and externally applied electromagnetic force.[31] At present, active targeting is considered necessary for the efficient uptake of drug in the tumor cells in addition to the EPR effect by passive targeting.

The combination of MB and US is one of the methods recently attracting attention in the field of gene introduction and drug delivery.[33-36] Through ultrasonic irradiation, MB tentatively change cell membrane transmission by sonoporation, enabling the uptake of extracellular high-molecular-weight substances without causing cell injury.[7-11,33-36] The cavitation effect caused by the collapse of bubbles is considered the key mechanism of drug delivery into cells. This technique has been experimented upon both in vitro and in vivo as a site-specific method of drug delivery.[7,12] However, MB have had the problem of difficulty in functional ligand attachment to the surface for targeting. We prepared BL from liposomes by a new method to solve this problem and succeeded in sealing perfluoropropane gas, which serves as a nucleus to cause cavitation in BL[20,37] and employed this new type of BL in this study.

Our in vitro results suggest that it is possible to significantly inhibit osteosarcoma cell growth by adding BL and US to DOX. In vitro setting, the EPR effect that observed in the tumor tissue of the living body is unlikely expected. Thus, this action mechanism is assumed to be realized purely with the drug uptake increase induced by sonoporation effect and cavitation. Tumor targeting by EPR effect can be expected in vivo in addition to the sonoporation and cavitation effects observed in vitro. In fact, the new DDS we have constructed achieved growth inhibition almost equivalent to that observed with monotherapy with DOX, though at about 1/5 the dose used in monotherapy. In the intratumoral concentration assay, DOX concentration increased to 1.5 times that in the control. This finding indicated that our new DDS could induce high concentrations of DOX and BL specifically in tumor by EPR effect, enabling the uptake of high-concentration DOX in tumor tissue via the cavitation and sonoporation induced by US irradiation to the tumor site (**Fig. 4B**). Though there is a report on another experiment using liposomal DOX of a significant increase in hepatic tissue concentration,[27] no significant difference was observed in hepatic tissue concentration in our new DDS in comparison with the DOX monotherapy group. In our system, DOX and BL were simply mixed rather than sealing DOX inside of liposomes. This is probably a reason for the decreased uptake of DOX by the RES. In our system, DOX was not sealed in liposomes. Therefore, compared with sealed DOX, the amount of delivery into RES with BL of the remaining DOX not delivered into the tumor may be small.

Reduction of adverse events is a large advantage of our new DDS. As regards side effects, no significant difference was

observed between the group treated with DOX at 1 mg/kg in combination with BL and US and the control group, while Hb and Plt values decreased in the DOX monotherapy group (at 5 mg/kg). Thus, concomitant treatment with DOX at 1 mg in combination with BL and US could achieve a tumor inhibitory effect equivalent to that observed with monotherapy with DOX at 5 mg and could also reduce side effects. By employing this method, which enables treatment at lower doses, the number of drop-outs from chemotherapy may be reduced, with improvement of prognosis.

Since this study was performed in an osteosarcoma model prepared in the back of mice, it was possible to directly irradiate tumors with US. However, the problem with clinical application of this method is how US irradiation is to be performed when osteosarcoma cells are present in the bone. According to the reports made up to present, when the US is applied for intracranial monitoring of cerebral blood flow after t-PA (tissue plasminogen activator) administration in acute ischemic stroke case, a thrombus dissolution effect reached 50% due to the ultrasonic action.[38,39] This finding suggests that US penetrated through cranial bone. Compared with transcranial Doppler (TED),[40] which is already in clinical use, the US used in the present study differs in frequency, strength and other factors. However, it should be possible to cause cavitation in the tissues of bones in the extremities with further research on US conditions. In the treatment of malignant tumor in the soft part of bone, externally infiltrating tumors are a serious problem. Since the tumors are soft part tumors, which are resistant to chemotherapy, our system seems to be a very effective option in the current treatment option of such tumor.

The 5-year survival rate of osteosarcoma has been stagnant in the past 10 years or more. A breakthrough is thus needed to drastically improve the results of treatment. The efficacy of anticancer drugs still holds the key to survival in current medical care. In this regard, the problems of lack of drug response and drug resistance need to be solved. Since powerful regimens prepared with combinations of existing anticancer drugs are still unable to markedly improve the results of treatment, it is necessary to develop a molecular targeting treatment whose mechanism is completely different from that of conventional anticancer drugs, and to create a method to increase the potency of existing anticancer drugs and at the same time reduce side effects by targeting of cancer cells as we have reported here. It is important that materials used in this method have been used safely in clinical treatment. The balance of risk and benefit is always the key issue when applying any treatment. BL and US are safe for the body, and it is possible with our method to perform location-specific treatment using a simple device. Although BL and US were used for treatment of osteorsarcoma in the present study, they are potentially applicable to treatment of some other malignant tumors as well. Accordingly, the method we have devised can be expected to be clinically useful.

Materials and Methods

Cell lines. The murine osteosarcoma cell line LM8 was obtained from RIKEN BioResource Center (Ibaraki, Japan). LM8, established from Dunn osteosarcoma, has high metastatic potential in the lung.[41] LM8 cells were cultured in the same fashion as reported previously in reference 41.

Preparation of liposomes and bubble liposomes. BL were prepared by the reverse-phase evaporation method in the same fashion as reported previously in reference 19. We prepared BL from liposomes by a new method to solve MB problem of difficulty in functional ligand attachment to the surface for targeting and succeeded in sealing perfluoropropane gas, which serves as a nucleus to cause cavitation in BL and employed this new type of BL in this study.

Regents. Doxorubicin (Doxorubicin hydrochloride) was purchased Sigma (St. Louis, MO).

Animal. C3H female mice (age, 4 weeks; weight, 16–20 g) were purchased from CLEA Co., Inc., (Tokyo, Japan). All mice were housed under specific pathogen-free conditions with a 12 h light/dark cycle. The housing care rules and experimental protocol were approved by the Guide for Animal Experimentation, Faculty of Medicine, Kagoshima University.

In vitro assay. *Cytotoxicity of BL and US to LM8 cells.* LM8 cells were collected with trypsin (Sigma-Aldrich) and washed twice with PBS. LM8 cells (14 x 10^4 cells), DOX (0.03 μg/μl) and BL (0.5%) mixed with 1,400 μl of culture medium in 2 ml polypropylene tubes (SUMITOMO BAKELITE, Tokyo, Japan) were exposed to US. A 6-mm diameter Sonopore KTAC-4000 probe (NEPA GENE CO., LTD., Chiba, Japan) was used for ultrasonic irradiation. The probe was inserted directly into the tubes and secured 3 mm above the bottom. US irradiation was performed at 1 MHz frequency using the following conditions: 0.5 w/cm^2 power density, 50% duty cycle, 10 sec duration. Cell suspensions (100 μl) were subsequently seeded onto flat-bottomed 96-well plates at a concentration of 1 x 10^4 cells/well and incubated for 24 h, 48 h and 72 h (**Fig. 5**). Cell viability was assayed using MTT [3-(4,5 sec-dimethylthiazol-2-yl)-2,5-diphenyl tetrazolium bromide] as described by Mosmann with minor modifications.[42]

In vivo assay. *Animal model.* Before starting all experiments, osteosarcoma-bearing mice were divided into eight groups and subjected to different modalities of administration. Before implantation of tumor cells, mice were anesthetized with diethyl ether (Nacalai Tesque, Kyoto, Japan) and shaved unilaterally on the back. Cell suspensions (200 μl) in PBS were injected subcutaneously in the back of mice with a 27-gauge needle, with 1 x 10^6 LM8 cells delivered. The inoculated mice were monitored every other day and experiments were initiated approximately 7–10 days after inoculation when tumors reached 5–7 mm in size. This day was considered day 0 and C3H mice were anesthetized with a combination of ketamine HCl (Ketalal, 50 mg/kg, i.p.) and medetomidine HCl (Domitor, 0.3 mg/kg, i.p.). Mice were then divided into eight groups and subjected to different modalities of administration as follows: Group 1, control (no treatment); Group 2, DOX (1 mg/kg); Group 3, DOX (1 mg/kg) + BL + US; Group 4, DOX (5 mg/kg); Group 5, DOX (1 mg/kg) + US; Group 6, BL; Group 7, US; Group 8, BL + US. DOX and BL preparations were administered i.v. via the tail vein and the total volume of DOX and BL was fixed at 10 ml/kg

body weight. Immediately after injection, in the sonically treated groups (Group 3, 5, 7 and 8), a 6-mm US probe was placed directly on the tumor surface and US was generated (power, 2 W/cm^2; frequency, 2 MHz; duty cycle, 50%; burst rate, 2 Hz; duration, 60 sec). This treatment was repeated three times, on days 0, 2 and 4. After treatment, mice were monitored every day. These animal models were used to examine tumor growth delay, for assay of pulmonary metastasis, evaluation of side effects and determination of survival rates.

Tumor growth delay. Mice of groups 1–8 were used in this study. Tumor growth was monitored every 2 days by measuring tumor volume with a digital caliper (repeated three times). It was estimated by measuring longitudinal cross-section diameter (L) and diameter in a transverse section (W) and using the following formula:[43] $TV = L \times W^2/2$.

The mice were humanely euthanized on day 21. Tumor tissues were collected for histopathologic examination. Tumor growth was normalized by dividing tumor volume on day X by the tumor volume measured on day 0. These mice were used for examination of antitumor effects (primary tumor growth).

Evaluation of side effect. In clinical use of DOX, almost all patients suffer myelosuppression or liver dysfunction. We therefore collected blood to evaluate side effects. Group 1–4 mice were used in this study. On day 9, for measurements of red blood cells (RBC), white blood cells (WBC), hemoglobin (Hb), platelets (Plt), glutamic-oxaloacetic transaminase (GOT) and glutamic-pyruvic transaminase (GPT), mice were anesthetized and 800 µl samples of blood were obtained from the inferior vena cava. At the time of blood collection, the liver was collected to confirm nonexistence of liver metastasis.

Assay for intratumoral DOX content. For further investigation, we estimated intratumoral DOX content. Mice with LM8 tumors of about 10 mm in diameter were used for this study. Either DOX (10 mg/kg) or DOX (10 mg/kg) + BL + US was administered as described above. At 5 min after drug administration, mice were sacrificed just prior to processing of tumors. The tumors of each of the mice were removed, after were after storage in liquid nitrogen homogenized with an ultrasonic disruptor. The homogenates were mixed with chloroform and isopropanol (1:1, 5 ml) and then centrifuged at 3,000 rpm for 5 min at 4°C and the supernatants were collected. Collected supernatants were centrifuged at 10,000 rpm for 5 min at 4°C again and the supernatants were collected as a sample. The level of fluorescence of each of the samples was obtained from the supernatants by fluorescence spectrophotometry and converted to DOX content. The DOX concentration of each sample was calculated according to the mass of the corresponding tumor.

Histology. In the tumor growth delay study, tumors from treated animals and from untreated animals as a control were dissected at the times specified in the Results, fixed with 10% buffered neutral formalin solution, and then embedded in paraffin as usual. Prepared sections were stained with H&E.

Statistical analysis. All values were expressed as means ± SEM. The Mann-Whitney U-test was used to determine the significance of differences in the tumor growth delay study. In the side effect study and intratumoral DOX concentration assay, Student's t-test was used to examine differences between experimental groups. The survival data were analyzed by Kaplan-Meier methods and survival periods were compared by the log-rank test. Findings of $p < 0.05$ were considered significant.

Acknowledgements

This work was supported by Grant-in-Aid for Scientific Research (KAKENHI: 22591662).

References

1. Arndt CA, Crist WM. Common musculoskeletal tumors of childhood and adolescence. N Engl J Med 1999; 341:342-52; DOI: 10.1056/NEJM199907293410507.
2. Bielack SS, Kempf-Bielack B, Delling G, Exner GU, Flege S, Helmke K, et al. Prognostic factors in high-grade osteosarcoma of the extremities or trunk: an analysis of 1,702 patients treated on neoadjuvant cooperative osteosarcoma study group protocols. J Clin Oncol 2002; 20:776-90; DOI: 10.1200/JCO.20.3.776.
3. Marina N, Gebhardt M, Teot L, Gorlick R. Biology and therapeutic advances for pediatric osteosarcoma. Oncologist 2004; 9:422-41; DOI: 10.1634/theoncologist.9-4-422.
4. Awada A, Piccart M. Strategies offering protection from the toxic effects of anticancer treatments with a focus on chemoprotective agents. Curr Opin Oncol 2000; 12:289-96; DOI: 10.1097/00001622-200007000-00003.
5. Meinardi MT, Gietema JA, van Veldhuisen DJ, van der Graaf WT, de Vries EG, Sleijfer DT. Long-term chemotherapy-related cardiovascular morbidity. Cancer Treat Rev 2000; 26:429-47; DOI: 10.1053/ctrv.2000.0175.
6. Greenleaf WJ, Bolander ME, Sarkar G, Goldring MB, Greenleaf JF. Artificial cavitation nuclei significantly enhance acoustically induced cell transfection. Ultrasound Med Biol 1998; 24:587-95; DOI: 10.1016/S0301-5629(98)00003-9.
7. Li T, Tachibana K, Kuroki M, Kuroki M. Gene transfer with echo-enhanced contrast agents: comparison between Albunex, Optison and Levovist in mice-initial results. Radiology 2003; 229:423-8; DOI: 10.1148/radiol.2292020500.
8. Shohet RV, Chen S, Zhou YT, Wang Z, Meidell RS, Unger RH, et al. Echocardiographic destruction of albumin microbubbles directs gene delivery to the myocardium. Circulation 2000; 101:2554-6.
9. Sonoda S, Tachibana K, Uchino E, Okubo A, Yamamoto M, Sakoda K, et al. Gene transfer to corneal epithelium and keratocytes mediated by ultrasound with microbubbles. Invest Ophthalmol Vis Sci 2006; 47:558-64; DOI: 10.1167/iovs.05-0889.
10. Taniyama Y, Tachibana K, Hiraoka K, Aoki M, Yamamoto S, Matsumoto K, et al. Development of safe and efficient novel nonviral gene transfer using ultrasound: enhancement of transfection efficiency of naked plasmid DNA in skeletal muscle. Gene Ther 2002; 9:372-80; DOI: 10.1038/sj.gt.3301678.
11. Taniyama Y, Tachibana K, Hiraoka K, Namba T, Yamasaki K, Hashiya N, et al. Local delivery of plasmid DNA into rat carotid artery using ultrasound. Circulation 2002; 105:1233-9; DOI: 10.1161/hc1002.105228.
12. Lindner JR. Microbubbles in medical imaging: current applications and future directions. Nat Rev Drug Discov 2004; 3:527-32; DOI: 10.1038/nrd1417.
13. Harata M, Soda Y, Tani K, Ooi J, Takizawa T, Chen M, et al. CD19-targeting liposomes containing imatinib efficiently kill Philadelphia chromosome-positive acute lymphoblastic leukemia cells. Blood 2004; 104:1442-9; DOI: 10.1182/blood-2004-02-0588.
14. Kawamura K, Kadowaki N, Suzuki R, Udagawa S, Kasaoka S, Utoguchi N, et al. Dendritic cells that endocytosed antigen-containing IgG-liposomes elicit effective antitumor immunity. J Immunother 2006; 29:165-74; DOI: 10.1097/01.cji.0000190169.61416.f5.
15. Kogure K, Moriguchi R, Sasaki K, Ueno M, Futaki S, Harashima H. Development of a non-viral multifunctional envelope-type nano device by a novel lipid film hydration method. J Control Release 2004; 98:317-23; DOI: 10.1016/j.jconrel.2004.04.024.
16. Maruyama K, Ishida O, Kasaoka S, Takizawa T, Utoguchi N, Shinohara A, et al. Intracellular targeting of sodium mercaptoundecahydrododecaborate (BSH) to solid tumors by transferrin-PEG liposomes, for boron neutron-capture therapy (BNCT). J Control Release 2004; 98:195-207; DOI: 10.1016/j.jconrel.2004.04.018.
17. Mizoue T, Horibe T, Maruyama K, Takizawa T, Iwatsuru M, Kono K, et al. Targetability and intracellular delivery of anti-BCG antibody-modified, pH-sensitive fusogenic immunoliposomes to tumor cells. Int J Pharm 2002; 237:129-37; DOI: 10.1016/S0378-5173(02)00044-3.
18. Suzuki R, Takizawa T, Kuwata Y, Mutoh M, Ishiguro N, Utoguchi N, et al. Effective anti-tumor activity of oxaliplatin encapsulated in transferrin-PEG-liposome. Int J Pharm 2008; 346:143-50; DOI: 10.1016/j.ijpharm.2007.06.010.
19. Suzuki R, Takizawa T, Negishi Y, Hagisawa K, Tanaka K, Sawamura K, et al. Gene delivery by combination of novel liposomal bubbles with perfluoropropane and ultrasound. J Control Release 2007; 117:130-6; DOI: 10.1016/j.jconrel.2006.09.008.

20. Suzuki R, Takizawa T, Negishi Y, Utoguchi N, Sawamura K, Tanaka K, et al. Tumor specific ultrasound enhanced gene transfer in vivo with novel liposomal bubbles. J Control Release 2008; 125:137-44; DOI: 10.1016/j.jconrel.2007.08.025.
21. Suzuki R, Oda Y, Utoguchi N, Namai E, Taira Y, Okada N, et al. A novel strategy utilizing ultrasound for antigen delivery in dendritic cell-based cancer immunotherapy. J Control Release 2009; 133:198-205.
22. Negishi Y, Endo Y, Fukuyama T, Suzuki R, Takizawa T, Omata D, et al. Delivery of siRNA into the cytoplasm by liposomal bubbles and ultrasound. J Control Release 2008; 132:124-30; DOI: 10.1016/j.jconrel.2008.08.019.
23. Negishi Y, Omata D, Iijima H, Takabayashi Y, Suzuki K, Endo Y, et al. Enhanced laminin-derived peptide AG73-mediated liposomal gene transfer by bubble liposomes and ultrasound. Mol Pharm 2010; 7:217-26; DOI: 10.1021/mp900214s.
24. Suzuki R, Namai E, Oda Y, Nishiie N, Otake S, Koshima R, et al. Cancer gene therapy by IL-12 gene delivery using liposomal bubbles and tumoral ultrasound exposure. J Control Release 2010; 142:245-50; DOI: 10.1016/j.jconrel.2009.10.027.
25. Allen TM, Hansen C, Martin F, Redemann C, Yau-Young A. Liposomes containing synthetic lipid derivatives of poly(ethylene glycol) show prolonged circulation half-lives in vivo. Biochim Biophys Acta 1991; 1066:29-36; DOI: 10.1016/0005-2736(91)90246-5.
26. Blume G, Cevc G. Liposomes for the sustained drug release in vivo. Biochim Biophys Acta 1990; 1029:91-7; DOI: 10.1016/0005-2736(90)90440-Y.
27. Klibanov AL, Maruyama K, Torchilin VP, Huang L. Amphipathic polyethyleneglycols effectively prolong the circulation time of liposomes. FEBS Lett 1990; 268:235-7; DOI: 10.1016/0014-5793(90)81016-H.
28. Matsumura Y, Maeda H. A new concept for macromolecular therapeutics in cancer chemotherapy: mechanism of tumoritropic accumulation of proteins and the antitumor agent smancs. Cancer Res 1986; 46:6387-92.
29. Muggia FM. Doxorubicin-polymer conjugates: further demonstration of the concept of enhanced permeability and retention. Clin Cancer Res 1999; 5:7-8.
30. Hoving S, Seynhaeve AL, van Tiel ST, Eggermont AM, ten Hagen TL. Addition of low-dose tumor necrosis factor-alpha to systemic treatment with STEALTH liposomal doxorubicin (Doxil) improved anti-tumor activity in osteosarcoma-bearing rats. Anticancer Drugs 2005; 16:667-74; DOI: 10.1097/00001813-200507000-00012.
31. Nobuto H, Sugita T, Kubo T, Shimose S, Yasunaga Y, Murakami T, et al. Evaluation of systemic chemotherapy with magnetic liposomal doxorubicin and a dipole external electromagnet. Int J Cancer 2004; 109:627-35; DOI: 10.1002/ijc.20035.
32. Shimose S, Sugita T, Nitta Y, Kubo T, Ikuta Y, Murakami T. Effect of thermosensitive liposomal doxorubicin with hyperthermia on primary tumor and lung metastases in hamster osteosarcoma. Int J Oncol 2001; 19:585-9.
33. Gordon AN, Fleagle JT, Guthrie D, Parkin DE, Gore ME, Lacave AJ. Recurrent epithelial ovarian carcinoma: a randomized phase III study of pegylated liposomal doxorubicin versus topotecan. J Clin Oncol 2001; 19:3312-22.
34. Sonoda S, Tachibana K, Uchino E, Yamashita T, Sakoda K, Sonoda KH, et al. Inhibition of melanoma by ultrasound-microbubble-aided drug delivery suggests membrane permeabilization. Cancer Biol Ther 2007; 6:1276-83; DOI: 10.4161/cbt.6.8.4485.
35. Kinoshita M, Hynynen K. A novel method for the intracellular delivery of siRNA using microbubble-enhanced focused ultrasound. Biochem Biophys Res Commun 2005; 335:393-9; DOI: 10.1016/j.bbrc.2005.07.101.
36. Kinoshita M, Hynynen K. Intracellular delivery of Bak BH3 peptide by microbubble-enhanced ultrasound. Pharm Res 2005; 22:716-20; DOI: 10.1007/s11095-005-2586-7.
37. Yamashita T, Sonoda S, Suzuki R, Arimura N, Tachibana K, Maruyama K, et al. A novel bubble liposome and ultrasound-mediated gene transfer to ocular surface: RC-1 cells in vitro and conjunctiva in vivo. Exp Eye Res 2007; 85:741-8; DOI: 10.1016/j.exer.2007.08.006.
38. Alexandrov AV, Molina CA, Grotta JC, Garami Z, Ford SR, Alvarez-Sabin J, et al. Ultrasound-enhanced systemic thrombolysis for acute ischemic stroke. N Engl J Med 2004; 351:2170-8; DOI: 10.1056/NEJMoa041175.
39. Molina CA, Ribo M, Rubiera M, Montaner J, Santamarina E, Delgado-Mederos R, et al. Microbubble administration accelerates clot lysis during continuous 2-MHz ultrasound monitoring in stroke patients treated with intravenous tissue plasminogen activator. Stroke 2006; 37:425-9; DOI: 10.1161/01.STR.0000199064.94588.39.
40. Aaslid R, Markwalder TM, Nornes H. Noninvasive transcranial Doppler ultrasound recording of flow velocity in basal cerebral arteries. J Neurosurg 1982; 57:769-74; DOI: 10.3171/jns.1982.57.6.0769.
41. Asai T, Ueda T, Itoh K, Yoshioka K, Aoki Y, Mori S, et al. Establishment and characterization of a murine osteosarcoma cell line (LM8) with high metastatic potential to the lung. Int J Cancer 1998; 76:418-22; DOI: 10.1002/(SICI)1097-0215(19980504)76:3<418::AID-IJC21>3.0.CO;2-5.
42. Mosmann T. Rapid colorimetric assay for cellular growth and survival: application to proliferation and cytotoxicity assays. J Immunol Methods 1983; 65:55-63; DOI: 10.1016/0022-1759(83)90303-4.
43. Martin F, Caignard A, Jeannin JF, Leclerc A, Martin M. Selection by trypsin of two sublines of rat colon cancer cells forming progressive or regressive tumors. Int J Cancer 1983; 32:623-7; DOI: 10.1002/ijc.2910320517.

Laboratory Investigation (2011), 1–14

NSAIDs inhibit neovascularization of choroid through HO-1-dependent pathway

Narimasa Yoshinaga[1], Noboru Arimura[1], Hiroki Otsuka[1], Ko-ichi Kawahara[2], Teruto Hashiguchi[2], Ikuro Maruyama[3] and Taiji Sakamoto[1]

Intraocular neovascularization is the leading cause of severe visual loss and anti-vascular endothelial growth factor (VEGF) therapy is currently performed for choroidal neovascularization (CNV). Despite its potent anti-angiogenic effect, there are concerns about its long-term safety. Non-steroidal anti-inflammatory drugs (NSAIDs) are common therapeutic agents used for treating inflammatory diseases, and their anti-stress effects are attracting attention now. We studied the effects of topical NSAIDs on CNV, focusing on anti-stress proteins. Cultured retinal pigment epithelium (RPE) cells were treated with NSAIDs: bromfenac, indomethacin, or vehicle control. Transcription factor NF-E2-related factor 2 (Nrf2) and its downstream anti-oxidant protein heme oxygenase (HO)-1 were assessed using western blot and immunohistochemistry. As a result, NSAIDs induced translocation of Nrf2 into the nucleus and the robust expression of HO-1 in a dose- and time-dependent manner. Flow cytometric analysis revealed that bromfenac inhibited H_2O_2-induced apoptosis in cultured RPE cells. Next, we studied the effects of topical bromfenac on laser-induced CNV model in rat. The expressions of Nrf2 and HO-1, infiltrations of ED-1-positive macrophages at CNV lesions and size were analyzed. VEGF in the ocular fluid of these rats was also measured using enzyme-linked immunosorbent assay. Rats administered an inhibitor of HO-1 stannic mesoporphyrin (SnMP) were also studied. The results showed that topical bromfenac led to translocation of Nrf2 and induction of HO-1 in CNV lesions and that the number of infiltrating macrophages at the CNV lesion decreased. The sizes of CNV lesions were significantly smaller in bromfenac-treated rats than control CNV, and the effects were diminished by SnMP. VEGF increased in the ocular fluid after laser treatment and was inhibited by bromfenac and SnMP canceling these effects. NSAIDs inhibit CNV through the novel anti-stress protein HO-1-dependent pathway, indicating its potential therapeutic value for various intraocular angiogenic diseases including CNV.

Laboratory Investigation (2011) **0,** 000–000. doi:10.1038/labinvest.2011.101

KEYWORDS: age-related macular degeneration; anti-VEGF; choroidal atrophy; photodynamic therapy; oxidative stress; steroid

Ocular angiogenesis such as choroidal neovascularization (CNV) is a leading cause of severe vision loss in patients with various ocular diseases.[1–3] Until recently, CNV was not a treatable condition and visual prognosis was poor. However, novel pharmacological therapies such as anti-vascular endothelial growth factor (VEGF) have revolutionized this field.[4,5] Despite significant advances, there are still concerns about the present anti-VEGF treatment. Complete blocking of VEGF is a logically correct method; however, it may induce retinal damage after a long period, because VEGF is a neurotrophic factor and has an important role in the retinal development and neuroprotection.[6,7] There are several reports showing that complete blocking of VEGF results in retinal degeneration in animals.[8,9] Indeed, unexplainable retinal atrophy was noted in some eyes with age-related macular degeneration (AMD) treated after several years of intense anti-VEGF therapy.[10]

Recently, it was reported that non-steroidal anti-inflammatory drugs (NSAIDs) inhibit CNV in animals and a large retrospective study found a reduced incidence of CNV in AMD patients taking aspirin.[11–17] The anti-inflammatory properties of NSAIDs are believed to reside in their ability to inhibit the activity of cyclooxygenase (COX). Indeed COX2 was shown to have a pivotal role in the expression of VEGF in

[1]Department of Ophthalmology, Kagoshima University Graduate School of Medical and Dental Sciences, Kagoshima, Japan; [2]Department of Laboratory and Vascular Medicine, Kagoshima University Graduate School of Medical and Dental Sciences, Kagoshima, Japan and [3]Department of Systems Biology in Thromboregulation, Kagoshima University Graduate School of Medical and Dental Sciences, Kagoshima, Japan
Correspondence: Professor T Sakamoto, MD, PhD, Department of Ophthalmology, Kagoshima University Graduate School of Medical and Dental Sciences, 8-27-1, Sakuragaoka, Kagoshima 890-8520, Japan.
E-mail: tsakamot@m3.kufm.kagoshima-u.ac.jp

Received 17 January 2011; revised 30 March 2011; accepted 28 April 2011

a CNV animal model.[18] However, NSAIDs have other biological actions that inhibit nuclear factor-κB (NF-κB), which has a central role in the expression of various pro-inflammatory mediators.[19] Nonetheless, the real mechanism whereby NSAIDs inhibit CNV is not fully understood.

Heme oxygenase-1 (HO-1) is an anti-stress protein. Not only its substrate, heme, but also various stressors such as oxidative stressors, ultraviolet irradiation, inflammatory cytokines, and heavy metals have been reported to induce HO-1 production.[20–22] HO-1 degrades heme to carbon monoxide (CO), free iron, and biliverdin. Biliverdin is subsequently converted into bilirubin by biliverdin reductase.[20–22] Bilirubin and biliverdin are potent antioxidants, and CO has an anti-apoptotic activity. Therefore, upregulation of HO-1 in cells makes the cells resistant to apoptosis induced by various stressors. It was recently reported that NSAIDs upregulate HO-1 production in some types of cell.[23–27] If this anti-stress effect were inducible with topical NSAIDs, it would be very beneficial to use NSAIDs for the treatment of angiogenesis, because they may inhibit both pathological angiogenesis and potential collateral damage related to treatment. This would be especially advantageous for angiogenic disorders of the central nervous system including CNV. In this study, we explore the influence of NSAIDs on the regulation of anti-stress proteins *in vitro* focusing on their anti-apoptotic action and further on their effects on CNV models *in vivo*.

MATERIALS AND METHODS

Cell Culture

All experiments *in vitro* were performed using ARPE-19, a human diploid retinal pigment epithelium (RPE) cell line, which is in many ways similar to RPE *in vivo* (American Type Culture Collections, Manassas, VA).[28] All cultures were fed twice weekly with Dulbecco's modified Eagle's medium: nutrient mixture F12, plus 10% (vol/vol) fetal bovine serum, 2 mM L-glutamine, and penicillin–streptomycin at 100 IU/ml. Cultures were incubated at 37 °C in 5% (vol/vol) CO_2 incubator and sub-cultured with 0.05% trypsin–EDTA (all products were obtained from Invitrogen-Gibco, Rockville, MD). Subconfluent cultures were trypsinized and seeded for the following experiments.

Western Blot Analysis of NF-E2-Related Factor 2 (Nrf2) and HO-1

ARPE-19 cells were subcultured on 6-cm tissue culture dishes. The cells were serum starved for 3 h and stimulated with the indicated concentration of indomethacine (Funakoshi, Tokyo, Japan), bromfenac (provided from Senju Pharmaceutical, Osaka, Japan) as NSAIDs, or dimethylsulfoxide (DMSO) as control for the indicated time. Nuclear and cytoplasmic extracts of cells were prepared using the Pierce NE-PER nuclear and cytoplasmic extraction kit (Pierce, Rockford, IL). They were subjected to 10% SDS–polyacrylamide gel electrophoresis and transferred to nitrocellulose membranes (GE Healthcare Bio-sciences KK, Piscataway, NJ) as with our previous methods.[28,29] Membranes were incubated with a blocking buffer containing 1% BSA and 5% non-fat milk in 25 mM Tris–HCl-buffered saline with 0.02% Tween 20 (TBST), followed by incubation with the respective primary antibodies (1:200; anti-Nrf2 rabbit polyclonal antibody, 1:500; anti-HO-1 antibody, 1:200; anti-β-actin goat polyclonal antibody, Santa Cruz Biotechnology Inc., CA) in TBST containing 1% non-fat milk overnight at 4 °C. After three washes with TBST, membranes were incubated with horseradish peroxidase (HRP)-conjugated anti-rabbit IgG polyclonal antibody (Santa Cruz Biotechnology Inc.) or HRP-conjugated anti-goat IgG polyclonal antibody diluted 1:3000 in TBST containing 2.5% non-fat milk for 1 h. The membrane was washed twice, and immunoreactive bands were visualized using an ECL detection system (GE Healthcare Bio-sciences KK). Immunoreactive bands were quantified and relative sum intensities of bands were compared using Image J Software (US National Institutes of Health).

Immunocytochemistry of Nrf2 and HO-1

Immunocytochemistry was carried out in accordance with our previous method.[28,29] ARPE-19 cells were grown on culture slides and serum starved for 3 h, then treated with the indicated concentration of indomethacin, bromfenac, or DMSO as the control for 3 h. After treatment, slides were washed with PBS, fixed with OptiLyse C (Beckman Coulter, Miami, FL), blocked with 1% BSA in PBS containing 0.1% of triton-X100 (PBST) for 60 min and incubated with polyclonal rabbit anti-Nrf2 and anti-HO-1 antibody (each 1:100; Santa Cruz Biotechnology Inc.) in PBS containing 1.5% BSA for 60 min at room temperature. The slides were washed with PBST, incubated with secondary antibodies, Alexa-Fluor 488-conjugated goat anti-mouse IgG F(ab)2 fragment, and Alexa-Fluor 594-conjugated goat anti-rabbit IgG F(ab)2 fragment (each 1:400; Molecular Probes, Carlsbad, CA) for an additional 60 min in the dark at room temperature. Stained cells were washed, mounted with Shandon Perma-Flour (Thermo Scientific, Waltham, MA), and examined with a Zeiss fluorescence microscope (Zeiss, Oberkochen, Germany).

Flow Cytometric Analysis

To analyze the cellular DNA content, the propidium iodide staining method was used as previously described. Briefly, ARPE-19 cells subcultured on 6-cm dishes at a density of 4.5×10^5 cells per dish and incubated with bromfenac or DMSO as a control were dissolved in medium with 1% fetal bovine serum for 24 h. After treatment for the indicated periods, the cells were washed with PBS. The pellet was resuspended in 70% ethanol (2 ml), and the suspension was incubated at −20 °C for 20 min. Cells were then incubated in the dark for 15 min with propidium iodide (5 g/ml) in PBS in the presence of RNase (5 g/ml). Then, the DNA content was

determined (2×10^4 cells each time) with a FACS analyzer (Epics; Beckman Coulter).

Cell Viability Assay

Cell viability was analyzed from mitochondrial respiratory activity measured using MTT (3-(4,5-dimethylthiazol-2yl)-2,5-diphenol tetrazolium bromide) assay (Wako Chemicals, Osaka, Japan), as described previously.[28] Briefly, 3.5×10^4 ARPE-19 cells were cultured in 24-well plates (500 ml medium per well) and pretreated with 2.5 μM bromfenac or DMSO dissolved in a medium with 1% fetal bovine serum for 24 h. Then, the cells were stimulated with or without hydrogen peroxide (500 μM; Merck, Darmstadt) for 15 min and incubated with MTT (0.5 mg/ml; final concentration) for 3 h. Formazan product was solubilized by the addition of DMSO for 16 h. Dehydrogenase activity was expressed as absorbance at a test wavelength of 570 nm and at a reference wavelength of 630 nm. Assays were performed in triplicate and repeated three times in independent experiments.

Animals

Brown-Norway rats (7 week old male; weight 140–160 g) were purchased from Kyudo (Fukuoka, Japan), and housed in a temperature-controlled room. The animals were kept on a 12-h light–dark schedule and had free access to food and water. All animals were treated in accordance with the ARVO Statement for the Use of Animals in Ophthalmic and Vision Research.

Induction of Experimental CNV

A rat CNV model was made accordance to our previous methods.[30,31] Briefly, rats were anesthetized with a 0.1–0.2 ml of a mixture of 100 mg/ml ketamine and 20 mg/ml xylazine. Pupils were dilated with a topical application of 5.0% phenylephrine and 0.8% tropicamide. CNV was experimentally produced with an argon dye-pulsed laser (Novus Varia, Lumenis, Salt Lake City, UT) and a slit lamp delivery system (SL-130; Carl Zeiss Meditec GmbH, Oberkochen, Germany) at a spot size of 100 μm, duration of 0.05 s, and intensity of 200 mW. Four laser photocoagulations were applied to each eye between the major retinal vessels around the optic disk under the previously described conditions.[30] The morphological end point of the laser injury was the appearance of a cavitation bubble, a sign that is thought to correlate with the disruption of Bruch's membrane. On occasion, the inducing laser burst created an extensive subretinal hemorrhage, and these spots were excluded from any further treatment or analysis.

Evaluation of Effects of Topical Bromfenac on Experimental CNV

A total of 20 male Brown-Norway rats were divided into saline-treated group and bromfenac-treated group. All rats underwent laser photocoagulation of the right eye as described above. Saline-treated group rats received eye drops of saline six times a day for 7 days. Drug administration was started the day after photocoagulation (day 1), and continued until day 7. Bromfenac-treated rats were received eye drops of human use bromfenac ophthalmic solution (Bronuk 0.1% ophthalmic solution, Senju Pharmaceutical) six times a day, for 7 days. The eyes were enucleated on day 8 and subjected to further examinations.

Choroidal Flat Mounts

Rats were anesthetized and perfused with 1 ml PBS containing 50 mg/ml fluorescein-labeled dextran (Sigma Aldrich, St Louis, MO) as previously described elsewhere.[12,13] After the eyes were enucleated and briefly fixed in 4% PFA, the anterior segment was removed and the retina was carefully dissected from the eyecup. Four to six radial cuts were made from the edge to the equator, and the eyecup was flat mounted with the sclera facing down and viewed with a Zeiss fluorescence microscope. Images were captured using the same exposure time for each comparative section, taken with a CCD camera, and the sizes of CNV lesions were measured using Image J.

Western Blot Analysis

Retina–choroid whole mounts were isolated and frozen at −80 °C within 2 min after enucleation. Retina–choroids were later ultrasonically homogenized and cytoplasmic protein extracts were isolated using a Pierce NE-PER nuclear and cytoplasmic extraction kit (Pierce) at 4 °C. The protein extracts (20 μg of protein in each lane) were subjected to the western blot analysis described above. For quantification, blots of five independent experiments were used.

Immunofluorescent Staining

Indirect immunofluorescent staining was carried out as described previously.[28,29] Enucleated eyes from the rats were immediately fixed in 4% paraformaldehyde at 4 °C for 12 h. The anterior segment and the lens were removed, and the remaining eyecup was cytoprotected with 10–30% sucrose in PBS. The eyecups were then frozen in an optimal cutting temperature compound (Sakura Finetech, Tokyo, Japan). Frozen sections (7 μm) were dried and blocked with blocking buffer for 1 h. The antibodies used for staining were rabbit polyclonal anti-Nrf2 antibody, rabbit polyclonal anti-HO-1 antibody (each 1:100; Santa Cruz Biotechnology Inc.), mouse anti-CD68 monoclonal antibody (ED1; 1:800; Serotec, Raleigh, NC), mouse anti-glial fibrillary acidic protein (GFAP) monoclonal antibody (1:400; Sigma Aldrich), mouse anti-RPE 65 monoclonal antibody, and mouse anti-CD31 monoclonal antibody (PECAM-1; 1:250 and 1:100, respectively; Abcam, Cambridge, UK). Normal rabbit or mouse IgG was used instead of primary antibody as a negative control in each case. Secondary antibodies were Alexa-Fluor 488-conjugated goat anti-mouse IgG F(ab)2 fragment and Alexa-Fluor 594-conjugated goat anti-rabbit IgG F(ab)2 fragment (each 1:400; Molecular Probes). Slides were

counterstained with DAPI, mounted with Shandon Perma-Fluor (Thermo Scientific), and viewed with a Zeiss fluorescence microscope. Images were captured using the same exposure time for each comparative section. For all experiments, at least three sections from each eye were evaluated. To quantify the macrophage infiltration, 10 different images were randomly selected by a controller (NY) and examined by masked observers (NA and HO).

Evaluation of Intraocular VEGF

We also measured concentrations of VEGF in the intraocular fluid (mixture of aqueous humor and vitreous fluid) as described previously with some modifications.[30] On day 8, the eyes were enucleated under deep anesthesia, the conjunctival tissue was removed, and the remaining eye tissues (cornea, iris, vitreous body, retina, choroids, and sclera) were collected in a tube and four to six radial cuts were made from the equator to cornea edge and to optic nerve at 4 °C. After centrifugation at 12 000 *g* for 30 s, supernatants were collected, and the concentrations of VEGF were measured using ELISA development kits (R&D Systems, Minneapolis, MN). VEGF concentration was adjusted by each protein concentration as previously described.[29] The adjusted concentration from a single eye was used as the concentration of VEGF.

Statistical Analysis

Because of the skewed distribution, the results were analyzed statistically using nonparametric tests (Mann–Whitney *U*-test) and were expressed as mean and range.

Statistical analyses were performed using SPSS software version 16.0 (SPSS Inc., Chicago, IL). A *P*-value of 0.05 was considered to be statistically significant. To adjust for inflated error resulting from multiple comparisons, the corrected significant *P*-value was defined as 0.05/4 using the Bonferroni correction for multiple comparisons.

RESULTS

NSAIDs Translocated Nrf2 and Upregulated HO-1 in Cultured RPE Cells

First, we examined whether transcriptional factor Nrf2 and phase 2 anti-oxidative protein HO-1 were expressed in ARPE-19 cells. Immunocytochemistry showed Nrf2 was located mainly in the cytoplasm and that HO-1 expression was barely detected in an untreated condition. After treatment with indomethacine or bromfenac, Nrf2 was translocated into the nucleus and HO-1 was abundantly present in the perinuclear lesion and cytoplasm (Figure 1).

Western blot analysis showed that treatment with indomethacine resulted in maximal immunoreactivity against Nrf2 at a concentration of 250 μM and 24 h of treatment, whereas HO-1 showed maximal band at a concentration of 50 μM, and this remained constant at 50–250 μM and showed maximal at 12 h of treatment. Treatment with bromfenac also showed maximal immunoreactivity for Nrf2 at a concentration of 160 μM. HO-1 showed maximal band at 40 μM and remained at 80 μM. Time-course examination showed maximal immunoreactivity at 12 h (Figure 2).

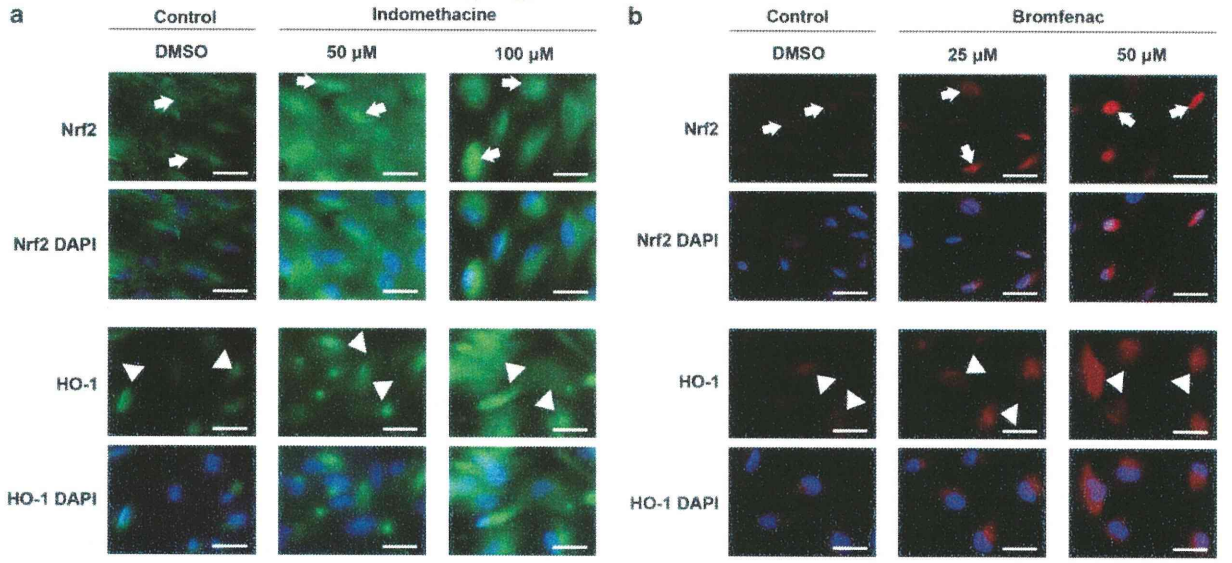

Figure 1 Expressions of Nrf2 and HO-1 protein in immunocytochemistry of ARPE-19 cells. (**a**) Treatment with the indicated concentration of indomethacine upregulated nuclear translocation of Nrf2. Nucleus was translucent or unstained in the control. On the other hand, Nrf2 was upregulated and nucleus is stained after indomethacine treatment (arrows). Cellular expressions of HO-1 were also upregulated in cytosol and nucleus (arrowheads). Scale bars: 30 μm. (**b**) Treatment with bromfenac also showed activation and increased Nrf2 expression in nucleus (arrows). Treatment with bromfenac increased the expression of HO-1 in nucleus and cytosol, especially around nucleus (arrowheads). Scale bars: 30 μm.

Bromfenac Inhibited RPE Cell Apoptosis Caused by Oxidative Stress

It has been reported that HO-1 has an anti-apoptotic property in human gastric mucosal cells.[32] We examined whether HO-1 induced by NSAIDs has functional properties against oxidative stress in ARPE-19 cells. H_2O_2 increased cell apoptosis in either DMSO-treated or bromfenac-treated cells ($15.6 \pm 4.01\%$ to $26.2 \pm 4.22\%$ in DMSO-treated control cells; $P<0.001$ *vs* $15.3 \pm 2.91\%$ to $20.3 \pm 3.02\%$ in bromfenac-treated cells; $P<0.005$). Apoptosis induced by oxidative stress was significantly less in bromfenac-treated cells compared with DMSO-treated control cells ($20.3 \pm 3.02\%$ bromfenac-treated cells *vs* $26.1 \pm 4.22\%$ DMSO-treated cells; $P<0.01$). Treatment with bromfenac itself resulted in no significant difference in apoptosis ($15.6 \pm 4.01\%$ DMSO-treated cells *vs* $15.3 \pm 2.91\%$ bromfenac-treated cells; $P=0.86$; Figure 3a and b).

We also tested cell viability in ARPE-19 cells using MTT assay. As described using propidium iodide staining and a FACS analyzer, H_2O_2 increased cell death of either DMSO-treated or bromfenac-treated cells (0% to $29.0 \pm 2.89\%$ in DMSO-treated control cells; $P<0.001$ *vs* $0.702 \pm 5.73\%$ to $23.5 \pm 4.04\%$ in bromfenac-treated cells; $P<0.001$). Cell death induced by oxidative stress was significantly less in bromfenac-treated cells compared with DMSO-treated control cells ($23.5 \pm 4.04\%$ bromfenac-treated cells *vs* $29.0 \pm 2.89\%$ DMSO-treated cells; $P<0.001$). Treatment with bromfenac itself made no significant difference to cell viability reduction (0% DMSO-treated cells *vs* $0.702 \pm 5.73\%$ bromfenac-treated cells; $P=0.519$;

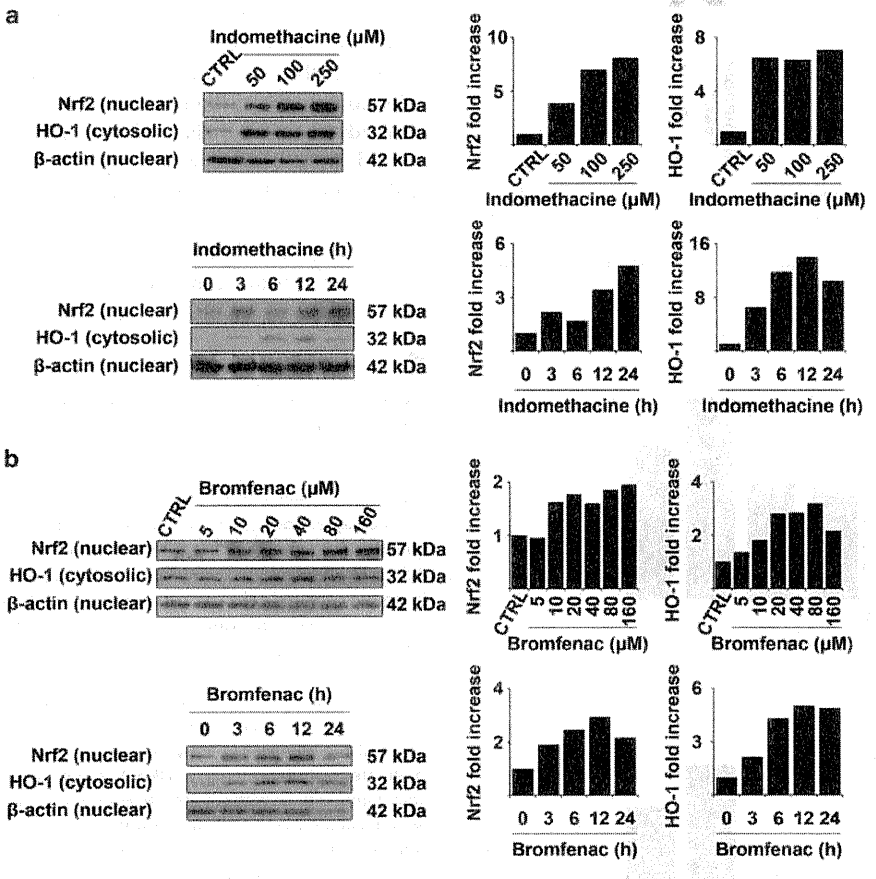

Figure 2 Nrf2 or HO-1 expression in ARPE19 cells by western blot analysis. (**a**; Top row) Serum-starved ARPE-19 cells were stimulated with indomethacine for 3 h and Nrf2 in nuclear protein and HO-1 in cytosolic protein were analyzed using western blots. Nrf2 in nuclear protein was increased by indomethacine in a dose-dependent manner. HO-1 in cytosolic protein is upregulated markedly with 50 μM indomethacine and this trend was continued through stimulation with 250 μM. (Bottom row) ARPE-19 cells were stimulated with indomethacine (250 μM) for the indicated time and subjected to the same analysis. Nrf2 in nuclear protein showed a time-dependent increase. On the other hand, HO-1 in cytosolic protein was showed maximal immunoreactivity at 12 h. (**b**; Top row) ARPE-19 cells were also stimulated with bromfenac for 3 h. Nrf2 was also upregulated in a dose-dependent manner. Increase of HO-1 in cytosolic protein was nearly the same as Nrf2 in nuclear protein. (Bottom row) Time-course expression of Nrf2 in nuclear protein and HO-1 in cytosolic protein with bromfenac (100 μM).

Figure 3c). Statistics were subjected to Mann–Whitney *U*-test with Bonferroni correction.

Reduction of Experimental CNV Size by Bromfenac in Rat Model

Our *in vitro* experiments showed that NSAIDs attenuated H_2O_2-induced RPE cell apoptosis. Next we examined the effects of bromfenac ophthalmic solution in a rat model of CNV. The size of CNV was measured with flat-mounted choroid stained with fluorescein dextran (Figure 4a). As shown in Figure 4b, CNV size was significantly smaller in bromfenac-treated eye ($32\,176 \pm 9165.1\ \mu m^2$) than in saline-treated rats ($48\,383 \pm 12\,733\ \mu m^2$; $P<0.001$, Mann–Whitney *U*-test).

Bromfenac Upregulated Nrf2 and HO-1 in Experimental CNV

The size of experimental CNV was reduced by topical bromfenac. To examine the underlying mechanism, we evaluated expressions of Nrf2 and HO-1 in the CNV area. Our results *in vitro* showed Nrf2 was strongly stained in cell nucleus especially at and adjacent to the CNV area in rats that received bromfenac compared with the control rats. At the same time, expression of HO-1 was observed in cells at CNV lesions. Notably, HO-1 was also strongly found not only at the CNV area but also in the entire retina (Figure 5a and b). To identify the cell type to express HO-1 in bromfenac-treated eyes, the eyes were double stained using anti HO-1 antibody and antibodies specific to each cell type. Anti-RPE65 antibody for RPE cells, anti-GFAP antibody for glial cells, anti-ED1 antibody for macrophages, and anti-CD31 antibody for endothelial cells in the rat CNV model were treated with bromfenac. HO-1 were obviously co-stained with RPE65, GFAP, ED1 antibodies (arrows), implying that RPE cells, GFAP-positive cells (astrocytes or Müller cells), and ED1-positive macrophages were strongly correlated with HO-1 production. HO-1 was also upregulated around

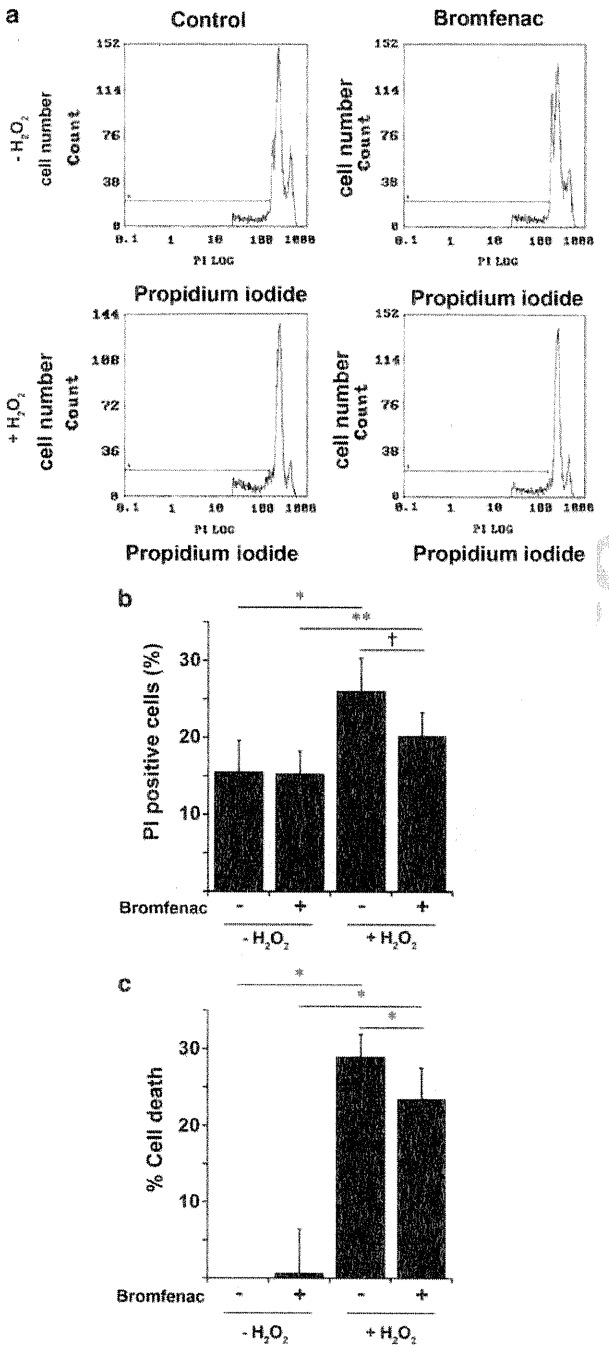

Figure 3 Anti-apoptotic effect of bromfenac was analyzed by flow cytometry. (**a**) ARPE-19 cells were pretreated with bromfenac (left lane) or DMSO (right lane) as a control for 24 h. Then, the cells were stimulated with (bottom) or without (top) 1 mM H_2O_2 for 3 h. After stimulation, the cells were stained with PI, and the DNA content was determined with a FACS analyzer. (**b**) H_2O_2 increased cell apoptosis in both DMSO-treated and bromfenac-treated cells (*$P<0.001$ and **$P<0.005$, respectively). Apoptosis induced by oxidative stress was significantly less in bromfenac-treated cells compared with DMSO-treated control cells ($^{\dagger}P<0.01$). Treatment with bromfenac itself resulted in no significant difference in apoptosis ($P=0.86$). Each group included results of 10 independent examinations ($n=10$). Data were expressed as mean ± s.e.m. The corrected significant *P*-value (Mann–Whitney *U*-test) was defined as 0.0125 (0.05/4 comparisons) after Bonferroni correction. (**c**) Cytoprotective effect of bromfenac was analyzed using MTT assay. ARPE-19 cells were pretreated with bromfenac or DMSO as control for 24 h. Then cells were stimulated with or without 500 μM H_2O_2 for 15 min. After stimulation, cells were incubated with MTT (0.5 mg/ml) for 3 h, formazan product was solubilized by DMSO, dehydrogenase activity was expressed as absorbance and % cell death was determined compared with control. H_2O_2 increased cell death in both DMSO-treated and bromfenac-treated cells (*$P<0.001$). Cell death induced by oxidative stress was significantly less in bromfenac-treated cells compared with DMSO-treated control cells (*$P<0.001$). Treatment with bromfenac itself made no significant difference in cell viability ($P=0.519$). ($n=16$). Data were expressed as mean ± s.e.m. The corrected significant *P*-value (Mann–Whitney *U*-test) was defined as 0.0125 (0.05/4 comparisons) after Bonferroni correction.

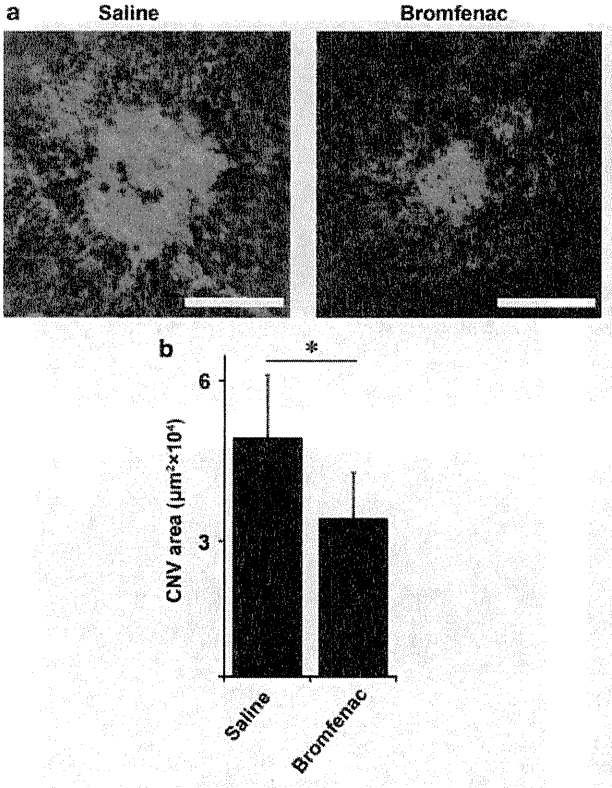

Figure 4 Size of CNV was examined after bromfenac treatment. (**a**) Representative CNV lesions of CNV flat mounts. Scale bars: 200 μm. (**b**) An analysis of the sizes of CNV lesions 8 days after PC. CNV size is smaller in bromfenac eye drop-treated rats 32 176 ± 9165.1 μm^2 than saline eye-drop treated rats 48 383 ± 12 733 μm^2 (*$P<0.001$, Mann–Whitney *U*-test). $n=40$ (40 PC spots of 10 rats). Data were expressed as mean ± s.e.m.

CD31-positive blood vessels, but less co-staining was observed compared with RPE cells or GFAP-positive cells (arrowheads; Figure 5c).

We also examined the protein quantity of Nrf2 and HO-1 using homogenates of retina and choroid of rat CNV model. Western blot analysis showed no immunoreactivity to Nrf2. It is more than probable that the concentration of Nrf2 in the prepared nuclear extract was too low to be detected. Western blot analysis of cytosolic extracts showed that HO-1 was upregulated in the tissue of rat treated with bromfenac as observed in immunohistochemical analysis (Figure 6a). An analysis using densitometry of five independent western blot results confirmed upregulation of HO-1 in bromfenac-treated eyes and photocoagulated (PC) eyes (Figure 6b). Expressions of HO-1 in saline-treated eyes with no PC were defined as base line, and fold increases of HO-1 in other eyes were calculated. Topical bromfenac significantly upregulated HO-1 expression (1.85 ± 0.19-fold, $P<0.01$), and bromfenac-treated eyes with PC expressed more significant HO-1 expression (2.21 ± 0.36-fold, $P<0.01$) compared with saline-treated eyes. Although there was no statistical significance, PC itself slightly upregulated HO-1 expression by 1.21 ± 0.24-fold).

HO-1 Inhibitor Stannic Mesoporphyrin (SnMP) Reversed Inhibitory Effect of Bromfenac on CNV

Upregulation of HO-1 by NSAIDs was observed both in our *in vitro* and *in vivo* experiments. We examined whether the inhibition of HO-1 changed the size of experimental CNV. Topical bromfenac decreased the size of CNV compared with the control (bromfenac rat 28 191 ± 5466 μm^2 *vs* control rat 42 405 ± 9004 μm^2 control: $P<0.001$). This inhibitory effect was diminished by intraperitoneal injection of SnMP (iSnMP; bromfenac rat 28 191 ± 5466 μm^2 *vs* bromfenac + iSnMP rats 44 677 ± 7619 μm^2, $P<0.001$ or control rat 42 405 ± 9004 μm^2 *vs* bromfenac + iSnMP rats 44 677 ± 7619 μm^2, $P=0.923$). On the other hand, iSnMP itself did not have any significant effect on CNV size (44 057 ± 14 775 μm^2; Figure 7).

Inhibitory Effect of Bromfenac on Macrophage Infiltration Was Diminished by SnMP

The above experiments revealed that topical bromfenac reduced the size of the CNV, and iSnMP reversed this reduction (Figure 8). To identify the mechanisms underlying this phenomenon, we measured the number of macrophages infiltrating into the CNV area. As a result, in the group which received intraperitoneal PBS (iPBS), infiltration of macrophage was significantly decreased in bromfenac-treated eyes compared with saline-treated eyes (18.0 ± 6.04 cells/field bromfenac + iPBS rats *vs* 32.4 ± 6.07 cells/field saline + iPBS rats; $P<0.01$). iSnMP reversed this effect and significantly increased macrophage infiltration (18.0 ± 6.04 cells/field bromfenac + iPBS rats *vs* 37.4 ± 4.28 cells/field bromfenac + iSnMP rats; $P<0.01$). There was no significant change with macrophage infiltration in saline-treated rats (31.0 ± 4.24 cells/field saline + iSnMP rats *vs*, 37.4 ± 4.28 cells/field bromfenac + iSnMP rats; $P=0.074$).

Reduction of Intraocular VEGF by Bromfenac Was Diminished by SnMP

The amount of VEGF in ocular fluid obtained from the CNV model on day 8 was evaluated with ELISA. As a result, the amount of VEGF increased in CNV model in comparison with rat eyes without laser burn. VEGF level was significantly lower in bromfenac-treated rat than control CNV rats (1.09 ± 0.88 pg/mg protein bromfena + iPBS rats *vs* 3.08 ± 3.19 pg/mg protein saline + iPBS rats; $P<0.01$). Additional iSnMP increased intraocular VEGF level as high as that of control CNV rats (5.35 ± 4.23 pg/mg protein bromfenac + iSnMP rats *vs* 1.09 ± 0.88 pg/mg protein bromfenac + iPBS rats; $P<0.001$). No significant difference resulted from iSnMP itself (4.09 ± 3.87 pg/mg protein saline + iSnMP rats *vs* 3.08 ± 3.19 pg/mg protein saline + iPBS rats; $P=0.499$; Figure 9).

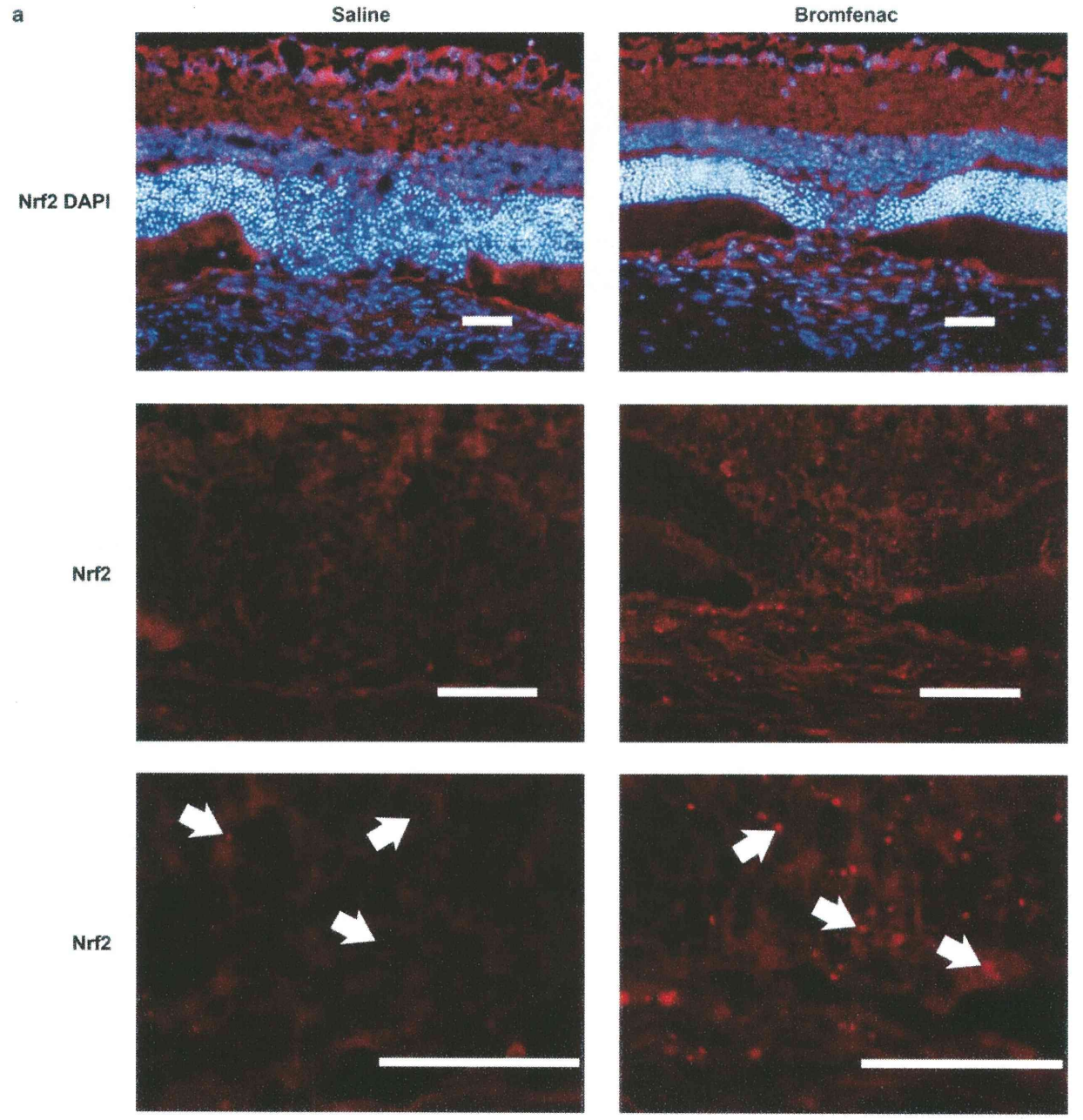

Figure 5 Immunohistochemical analysis was carried out for CNV lesions using Nrf2 or HO-1 protein. Immunofluorescent study was performed with anti-Nrf2 antibody (**a**) and anti-HO-1 antibody (**b**) in rat CNV model. Nuclei were counter-stained with 4′-6-diamidino-2-phenylindole (DAPI). (**a**) The results showed that expression of Nrf2 was upregulated and accumulated in cell nuclear especially at and near the CNV lesion (arrows). (**b**) Expression of HO-1 was also upregulated with bromfenac eye drop compared with saline-treated eye, especially at the photocoagulated CNV area and inner limited membrane (arrowheads). Scale bars: 100 μm. (**c**) Double staining for immunohistochemical analysis with anti-HO-1 antibody and cell-specific antibodies. Anti-RPE65 antibody for RPE cells, anti-GFAP antibody for glial cells, anti-ED1 antibody for macrophages, and anti-CD31 antibody for endothelial cells were in rat CNV model treated with bromfenac. HO-1 were obviously co-stained with RPE65, GFAP, ED1 antibodies (arrows), implying that RPE cells, GFAP-positive cells (astorcytes or Müller cells) and ED1-positive macrophages were strongly correlate with HO-1 production. HO-1 was also upregulated around CD31-positive blood vessels but less co-staining was observed compared with RPE cells or GFAP-positive cells (arrowheads). Nuclei were counter stained with DAPI. Scale bars: 100 μm.

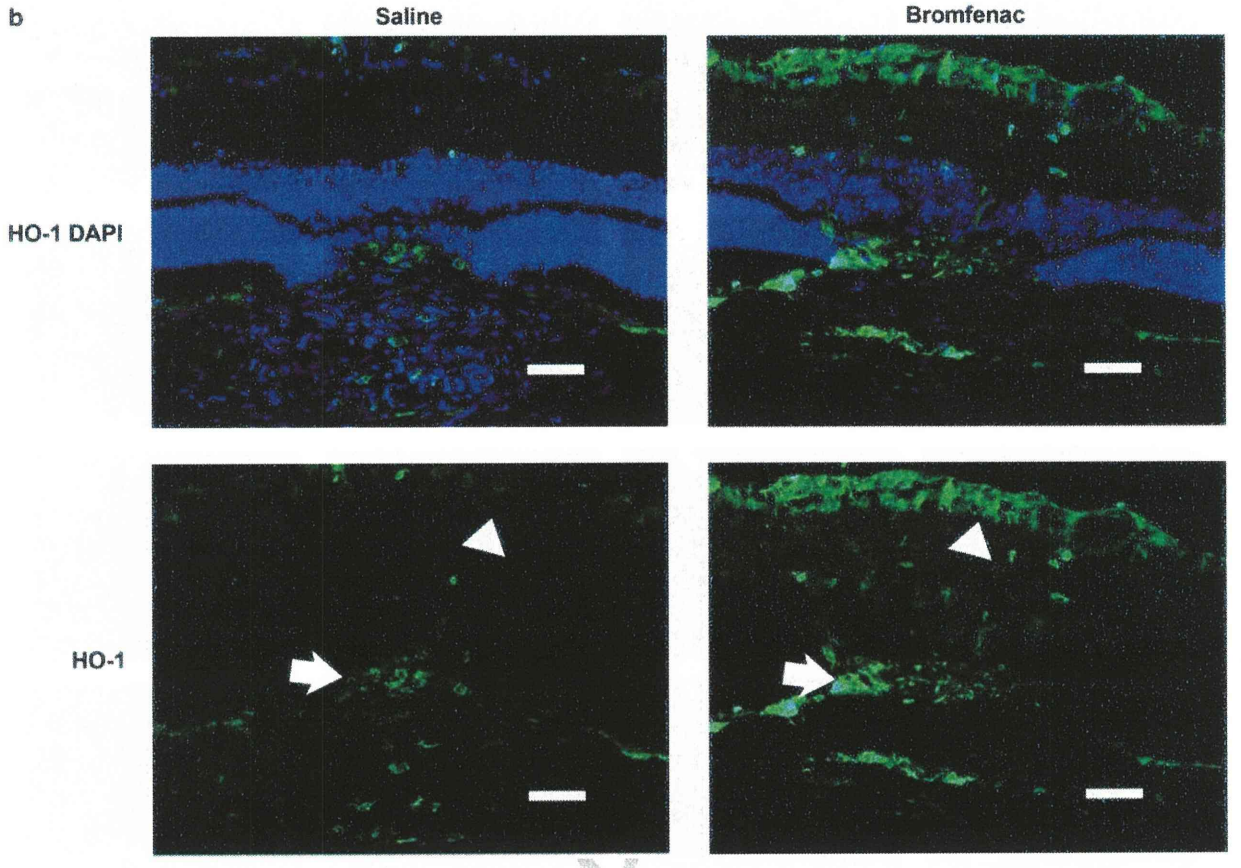

Figure 5 Continued.

DISCUSSION

Previously, we reported that intravitreous NSAIDs inhibited laser-induced CNV in sub-human primate; however, its mechanism was not well addressed.[11] Several recent reports showed possible mechanisms of the inhibitory effect of NSAIDs on CNV.[11–18] VEGF is one of the most potent molecules in angiogenesis. Takahashi *et al*[13] reported that nepafenac inhibited neovascularization in mice with CNV due to laser-induced rupture of Bruch's membrane and Kim *et al*[16] showed that ketrolac reduced the size of laser-induced CNV. Both suggested that the inhibitory effect of NSAIDs was due to downregulation of VEGF expression in the retina. Our previous study showed that blocking VEGF by gene transfer strongly inhibited CNV in this model.[31] Indeed, intraocular VEGF was significantly reduced in bromfenac-treated eyes in this study and thus inhibition of VEGF was also likely to have a crucial role in the inhibition of CNV formation found in this study.

There may be several explanations for the mechanism of this phenomenon. The first is the direct effect of NSAIDs on endothelial cells. It was reported that NSAIDs directly affect endothelial cells to down-regulate VEGF *in vitro*.[33,34] The targeted portions were supposed to be MAP kinase, ERK2 or the expression of VHL tumor suppressor protein, resulting in ubiquitination and degradation of HIF-1α.[33,34] Another report showed that NF-κB, which can also increase the expression of VEGF, and was inhibited by NSAIDs.[35] These direct mechanisms were probably at work in the present model, at least in part. The second is that the present phenomenon was caused by the inhibition of inflammation, which is an indirect effect. This explanation would be quite understandable because inflammatory cells are major sources of VEGF and depletion of macrophage strongly reduced the size of CNV, as demonstrated by ourselves and others.[36] NSAIDs were reported to reduce the prostaglandin, which is a known potent inducer of inflammation, in mouse retina.[14,16] Besides, NF-κB has a central role in the expression of various pro-inflammatory mediators and leukocyte infiltration.[37] So inflammation was inhibited by NSAIDs, consequently reducing the size of CNV. This is compatible with the present result that the number of macrophages infiltrating into the laser burned areas was significantly less in bromfenac-treated eyes than in PBS-treated controls.

In contrast, we shed light on another mechanism of NSAIDs in this study, ie, anti-stress protein in NSAIDs-mediated CNV suppression. Nrf2 is located at the cytosol binding to Keap1 under a stress-free condition; whereas after activation under the stressors, Nrf2 translocates to the

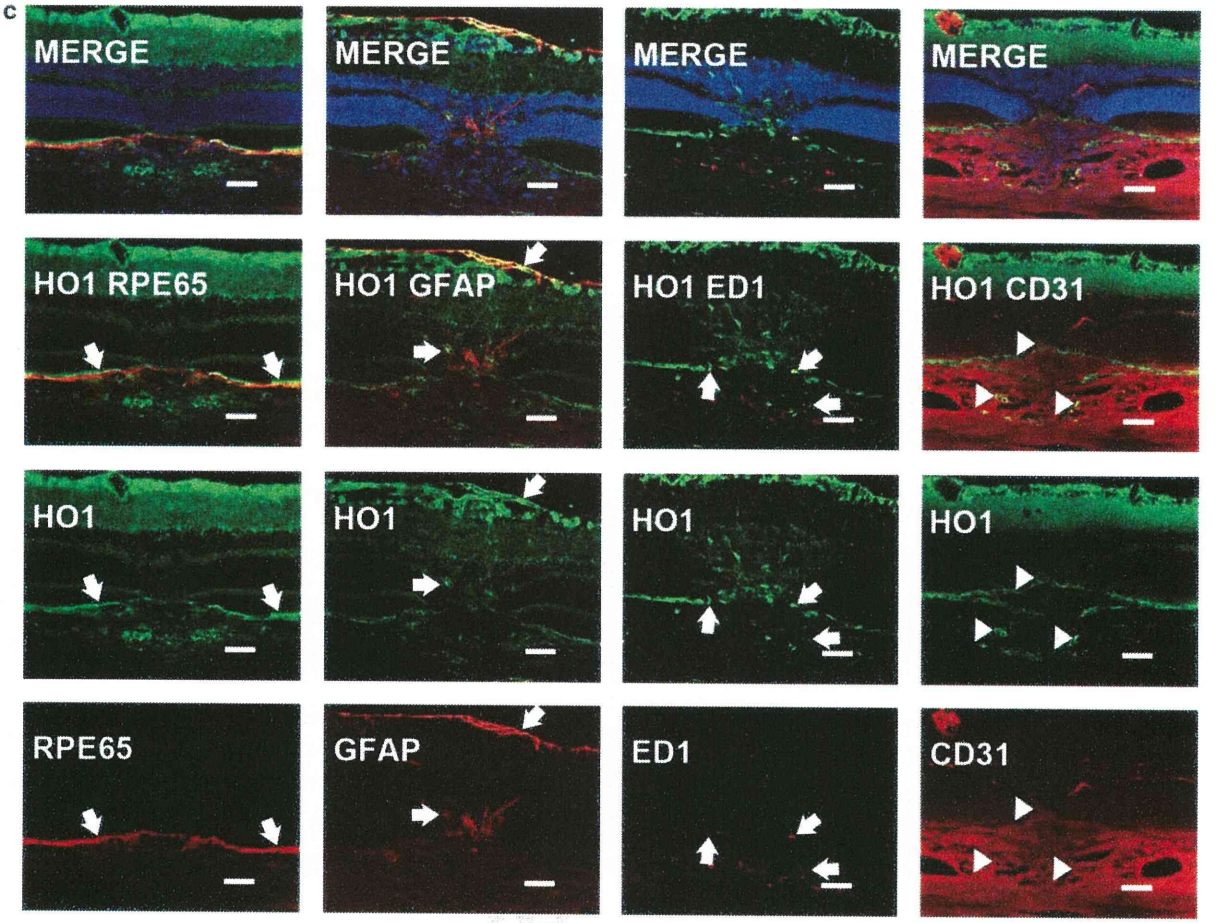

Figure 5 Continued.

nucleus, where it binds to the consensus *cis*-element (Maf-recognition element) to turn on the anti-oxidative stress mechanism, which can result in cell protection.[38,39] Because COX2 inhibits the activity of Nrf2, NSAIDs are supposed to activate the Nrf2/ARE pathways.[39,40] HO-1 is a phase II drug-detoxifying enzyme, such enzymes are regulated in a coordinated manner through a consensus *cis*-element and transcription factors, such as Nrf2. The present findings *in vitro* are consistent with this theory.

To our knowledge, this is the first report to show that NSAIDs induce HO-1 in the retina *in vivo* and *in vitro*. Interestingly, photocoagulation itself increased HO-1 expression in the retina, suggesting that HO-1 was induced by stress such as photocoagulation. However, HO-1 increased in bromfenac-treated eyes with no laser treatment and it was far more significant than in eyes with laser-burn alone. It is noteworthy that the inhibitory effect of bromfenac on CNV was diminished after the administration of SnMP. On the other hand, the size of CNV was not affected by saline eye drops after SnMP administration. These findings suggest that HO-1 does not necessarily have a pivotal role in CNV formation, but has a critical role in the inhibitory processes of bromfenac.

The role of HO-1 in angiogenesis is controversial.[41–43] It is suggested that during inflammation HO-1 has two different roles: first, an anti-inflammatory action inhibiting leukocyte infiltration; and second, promotion of VEGF-driven non-inflammatory angiogenesis, which facilitates tissue repair. In this study, bromfenac increased the expression of HO-1 associated with the inhibition of macrophage infiltration, whereas the inhibition of HO-1 by SnMP significantly augmented macrophage infiltration even in bromfenac-treated eyes. Thus, the increase of HO-1 expression by bromfenac was likely to lead to the inhibition of macrophage infiltration more than the promotion of VEGF-driven non-inflammatory angiogenesis in rat CNV model. Besides, our examination using intraocular fluids revealed that, bromfenac reduced the intraocular VEGF level (Figure 9). Consequently, CNV was inhibited.

Another important impact of HO-1 on retinal cells is its protective role, which was also observed as in the present *in vitro* study. In the *in vivo* study for example, curcumin

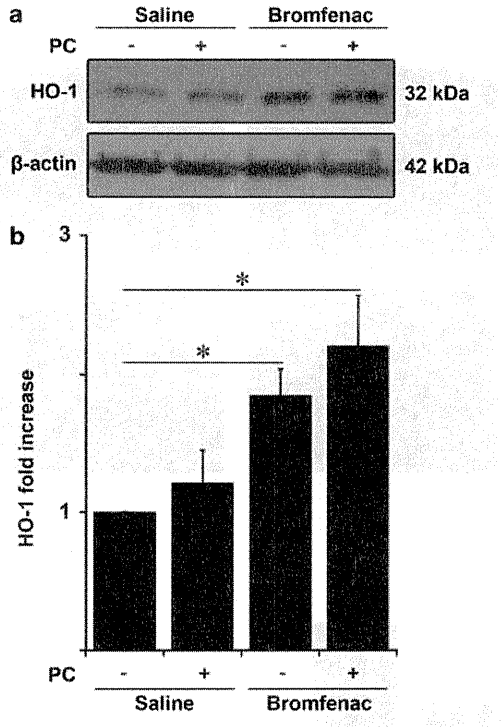

Figure 6 Western blot analysis of HO-1 in cytosolic proteins of rat retina–choroid homogenates. (**a**) Western blot shows HO-1 was upregulated with bromfenac and it was also slightly upregulated in eyes that received photocoagulation (PC) compared with others. (**b**) An analysis using densitometry on five independent western blots confirmed upregulation of HO-1 in bromfenac-treated eyes and photocoagulated eyes. Expressions of HO-1 in saline-treated eyes with no PC were defined as the base line, and fold increases of HO-1 in other eyes were calculated. Topical bromfenac significantly upregulated HO-1 expression ($^*P<0.01$), and bromfenac-treated eyes with PC expressed more significant HO-1 expression ($^*P<0.01$) compared with saline-treated eyes. Although not statistically significant, PC itself slightly upregulated HO-1 expression. The corrected significant *P*-value (Mann–Whitney *U*-test) was defined as 0.0125 (0.05/4 comparisons) after Bonferroni correction. Data were expressed as mean ± s.e.m.

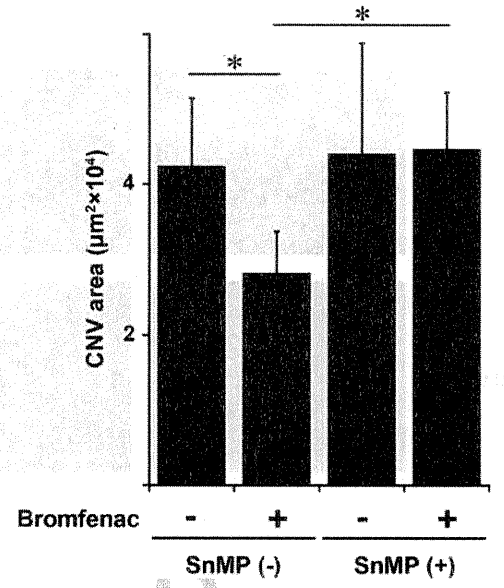

Figure 7 Effects of SnMP on inhibition of bromfenac over CNV size were studied. Topical bromfenac decreased the size of CNV compared with the control (bromfenac rat *vs* control rat. $^*P<0.001$ or bromfenac rat *vs* bromfenac + SnMP rat; $^*P<0.001$). This inhibitory effect was diminished by an inhibitor of HO-1 SnMP (control rat *vs* bromfenac + SnMP rats; $P=0.923$). On the other hand, SnMP itself did not have any significant effect on CNV size. The corrected significant *P*-value (Mann–Whitney *U*-test) was defined as 0.0125 (0.05/4 comparisons) after Bonferroni correction. $n=20$ (PC spots of five rats). Data were expressed as mean ± s.e.m.

protects retinal cells from light- or oxidant stress-induced cell death through the induction of HO-1.[44] Overexpression of HO-1 by gene transfer also inhibited light-induced photoreceptor cell apoptosis through Bcl-2 upregulation.[45] There are other reports showing that the induction of HO-1 by various stimulants rescued the retina in an ischemia-reperfusion model.[46] Therefore, NSAIDs might be beneficial for the treatment of CNV beyond their anti-angiogenic effect. This is especially true for the treatment of diseases of central nervous tissue including eye. At present, regeneration of neural tissue is clinically still difficult. Even if angiogenesis were to be blocked by an anti-VEGF drug, it would not necessarily mean the tissue function is protected. We need a potent angiogenesis therapy, but it must protect the host tissue as well. NSAIDs might be reasonable candidate drugs for this purpose.

It should be noted that there are other mechanisms to protect the retina from oxidative stress. Qin *et al*[47] showed that cyclopentenone 15-deoxy-delta^{12,14}-prostaglandin J2 protects RPE cells from oxidative injury. Although this mechanism is not evaluated in the present study, it is highly probable that these factors as a whole resulted in the present phenomenon.

There are different kinds of NSAIDs available. Each has different characteristics related to ocular penetration and inhibitory activity of COXs. For example, topical administration of 0.1% nepafenac inhibits the synthesis of PGs in the retina–choroid by 55% for 4 h.[48] Although, topical bromfenac has good ocular penetration and reaches a sufficient level in the retina and choroid, the inhibitory activity of bromfenac on either COX-1 or COX-2 was stronger than nepafenac or dicrofenac.[49,50] In our pilot study, we tested several different NSAIDs and found that topical bromfenac had a sufficient inhibitory effect on CNV in rat, as expected. Therefore, we chose bromfenac for the present study. But, it should be noted that the present results can be applied to bromfenac.

The present study has limitations. The present CNV model does not perfectly reflect clinical conditions. Certainly AMD or high myopia is a chronic and long-lasting disease. On the other hand, the present model is an acute wound-healing

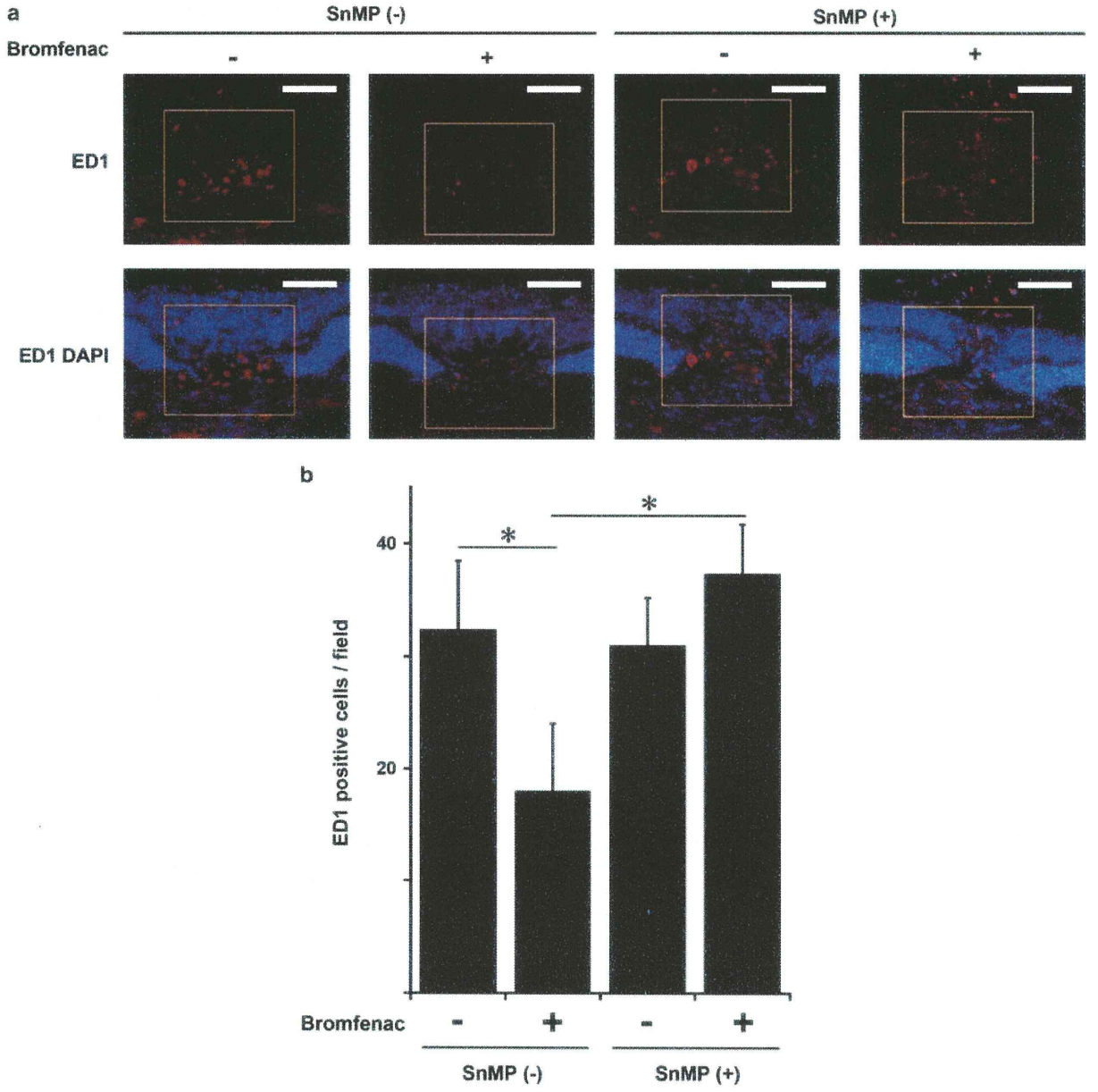

Figure 8 The number of infiltrating ED1-positive macrophages in CNV lesions was examined. (**a**) Representative images of rat CNV lesion identified by immunofluorescence with anti-ED1 antibody (red) and DAPI (blue). Scale bars: 150 μm (**b**). The number of ED1-positive macrophage infiltration expressed mean ± s.e.m. cells/field. In the group that received intraperitoneal PBS, infiltration of macrophage was decreased more significantly in bromfenac-treated rats than saline-treated rats ($^*P < 0.01$). Intraperitoneal injections of SnMP reversed this effect and significantly increased macrophage infiltration ($^*P < 0.01$). There was no significant change with macrophage infiltration in saline eye drop-treated rats ($P = 0.074$). $n = 10$. The corrected significant *P*-value (Mann–Whitney *U*-test) was defined as 0.0125 after Bonferroni correction. Square indicates CNV lesion.

model rather than a chronic disease model. Nonetheless, CNV in humans occurs in a similar manner to angiogenesis processes in acute wound healing and the present results will help an understanding of the clinical CNV. The second is that we measured the protein level of HO-1, but not its activity. The amount of protein does not necessarily reflect its biological activity. But the fact that an inhibitor of HO-1 reversed the effects of bromfenac indicates that HO-1 is likely to have played a major role in inhibiting CNV by bromfenac. The third is the treatment efficacy of NSAIDs. The current intravitreous anti-VEGF therapy is so potent for inhibiting CNV that there may be concerns that any new treatment will hardly improve on the current anti-VEGF therapy. However, complete blocking of VEGF might be potentially harmful